μSR による物性研究

Muon Spin Rotation
Relaxation
Resonance

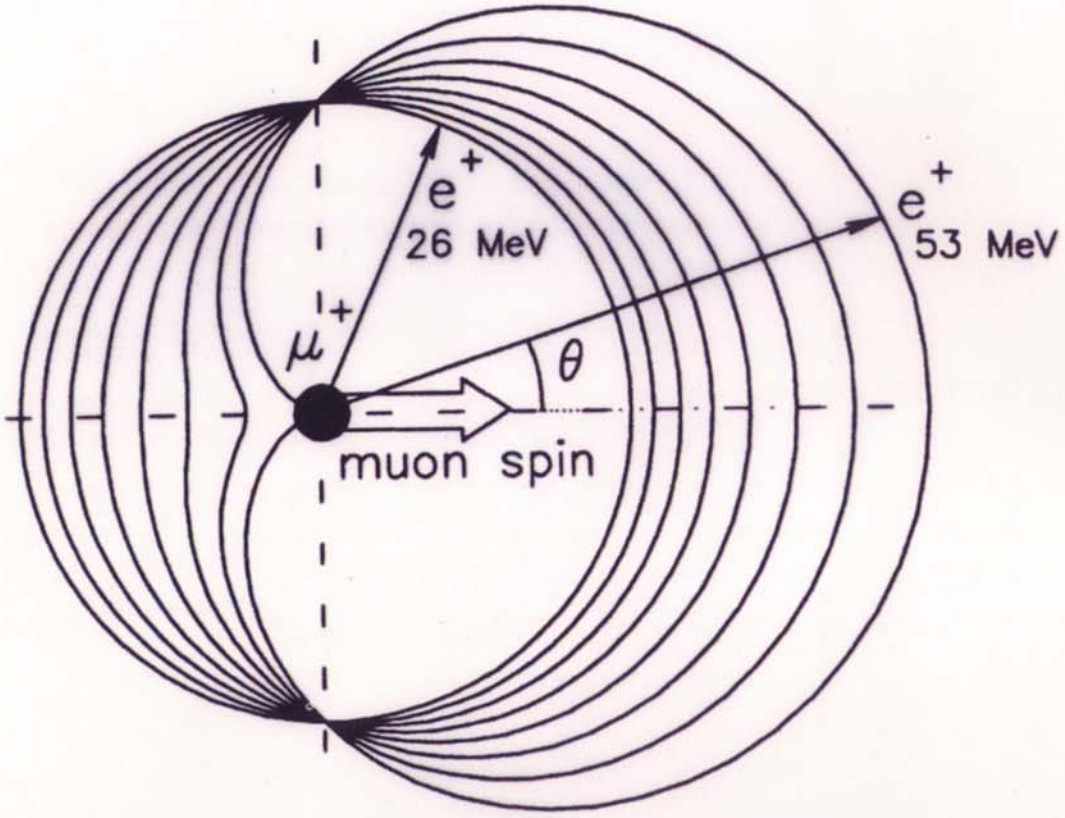

東京工業大学　物性物理学専攻
西田信彦

TIT　　Nobuhiko Nishida

μSRのはじまり

1957 Parity – non-conservation (^{60}Co C.S. Wu)

$\pi^+ \longrightarrow \mu^+ + \nu_\mu$ $\quad$ $\mu^+ \longrightarrow e^+ + \nu_e + \bar{\nu}_\mu$

$\pi^- \longrightarrow \mu^- + \bar{\nu}_\mu$ $\quad$ $\mu^- \longrightarrow e^- + \bar{\nu}_e + \nu_\mu$

- polarized μ spin, anisotropic emission of $e^\pm$ (Garwin, Ledermann, Weinrich) $1 + A\cos\theta$
- magnetic moment μ → $g_\mu \sim 2.0$

μ^+: Carbon target $A \sim 0.3$ → Nuclear Emulsion small A.

μ^-: small A → solid state effect

物性研究への応用が述べられている.

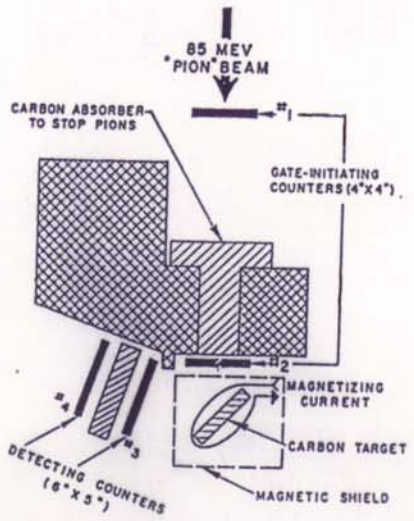

FIG. 1. Experimental arrangement. The magnetizing coil was close wound directly on the carbon to provide a uniform vertical field of 79 gauss per ampere.

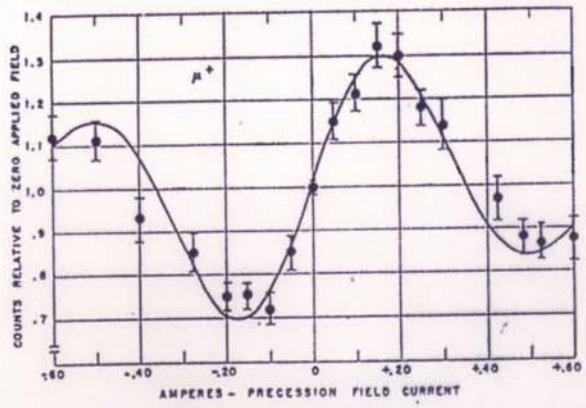

FIG. 2. Variation of gated 3–4 counting rate with magnetizing current. The solid curve is computed from an assumed electron angular distribution $1-\frac{1}{3}\cos\theta$, with counter and gate-width resolution folded in.

Phys. Rev. 105 (1957) 1415.

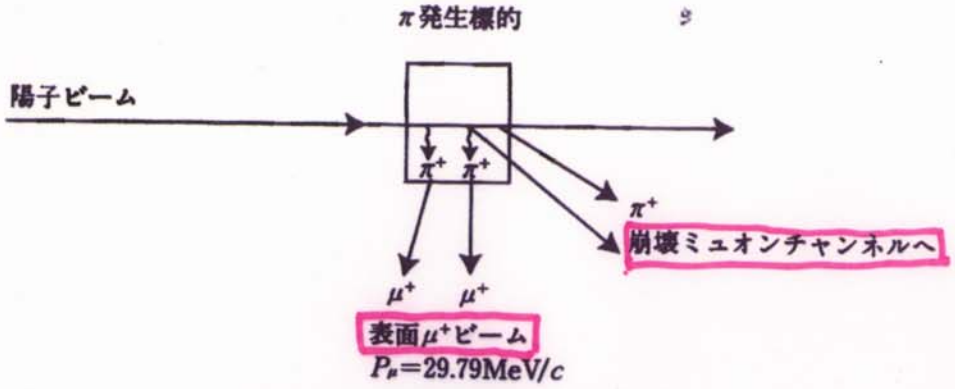

図 2.60　表面 μ^+ ビームの概念図

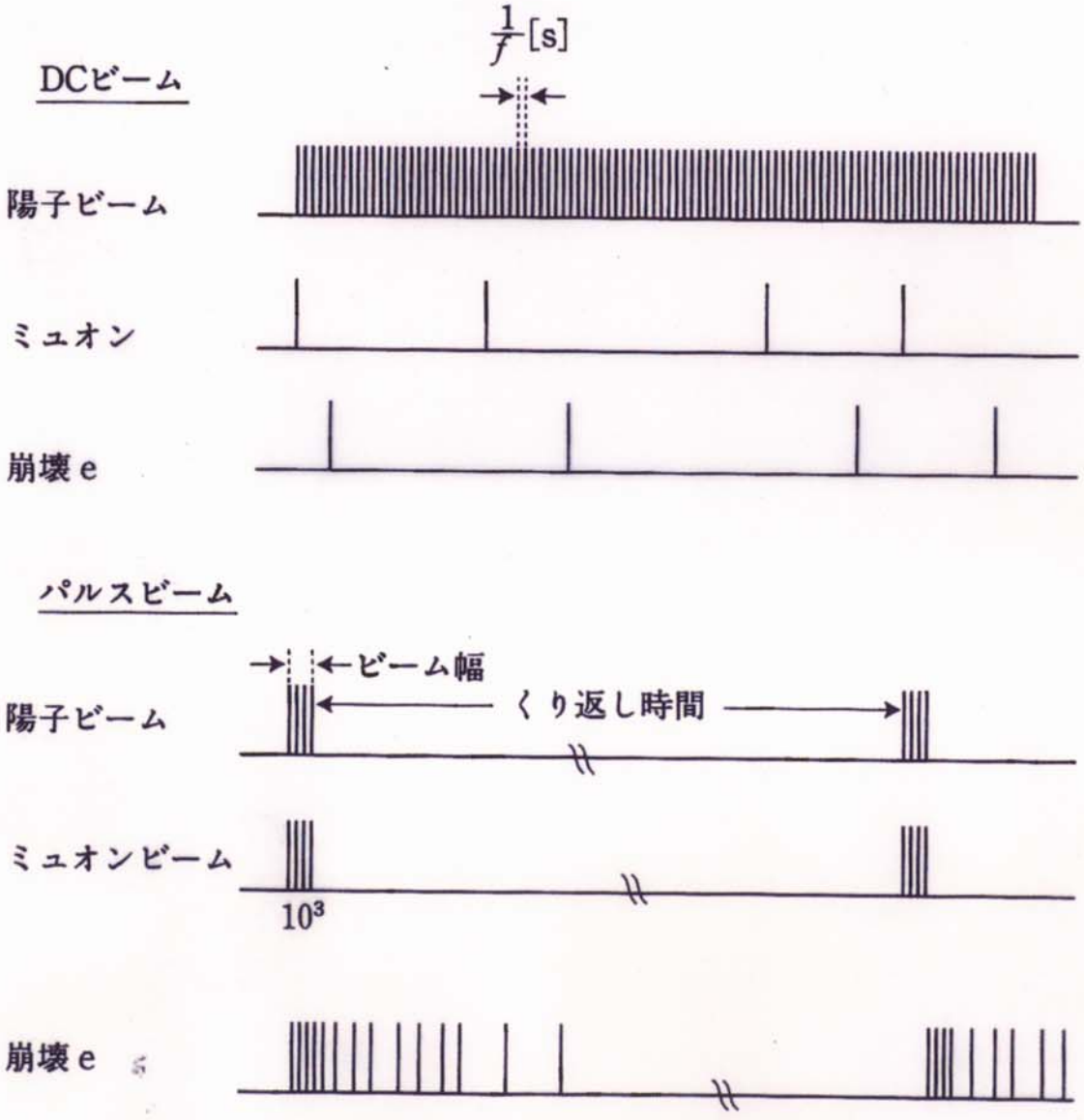

図 2.58　DC ビームとパルスビームの時間構造

統合計画：パルス
$10^{6/7}$/s

BOOM ：パルス
ダイオネガ Nagamine
10^5/s

PRISM
$10^{11\sim12}$/s
中：100ns
100Hz.

表 2.4

施設	μチャネル	時間構造		μの運動量 [MeV/c]	偏極[%]	μビームサイズ [cm²]	ルミノシティ		ストッピングレンジ [g/cm²]
		パルス幅	くり返し時間				μ^+[1/cm²·s]	μ^-[1/cm²·s]	
BOOM (2μA/パルス)	μ1(d)	50ns	50ms	6.5~110	~80	25	2×10^3	$\sim10^3$	1~3
	π1(s)			28	100	25	4×10^2	—	<0.05
RAL (200μA/パルス)	MuSR(s)	70ns	20ms	28	100	6	$\sim10^5$	—	<0.05
	EMU(s)			28	100	6	$\sim10^5$	—	<0.05
	DEVA(s)			28	100	6	$\sim10^5$	—	<0.05
	Port 1 (d/s)			27/50~80	100/80	6	$\sim10^5$(s)	10^4(d)	0.1/2
	Port 2 (d/s)			27/50~80	100/80	6	$\sim10^5$(s)	10^4(d)	0.1/2
	Port 3 (d/s)			27/50~80	100/80	6	$\sim10^5$(s)	10^4(d)	0.1/2
TRIUMF (140μA)	M 15(s)	DC	DC	28	100(⊥)	5	$\sim10^5$	—	~0.02
	M 9 B(d)			10~40	80	5		$\sim10^4$	1~2
	M 20 A(d)			80	80	20	3×10^4		2
	M 20 B(s)			28	100	20	1.6×10^4	—	~0.02
	M 13(s)			28	100	5	3×10^4	—	~0.02
PSI (1.5mA)	πM 3	DC	DC	10~300	>95	6	10^6 @28 MeV/c	10^6 @100 MeV/c	3×10^{-3}~80
	μE 4			30~100	75	24	2.5×10^5 @50MeV/c	6×10^4 @50 MeV/c	0.13~7
	μE 1			40~125	75	10	3×10^7 @125 MeV/c	9×10^6 @125 MeV/c	0.3~13
	πE 3			10~250	>95	7.5	10^7 @28 MeV/c	10^7 @100 MeV/c	3×10^{-3}~60

• ultra slow μ^+ ： 数 10 eV~30 keV
表面物理

10^4/s ：PSI
10^8/s → 10^{-4} の収率.

高エネルギー物理学研究所
中間子科学研究施設

中間子第一実験室

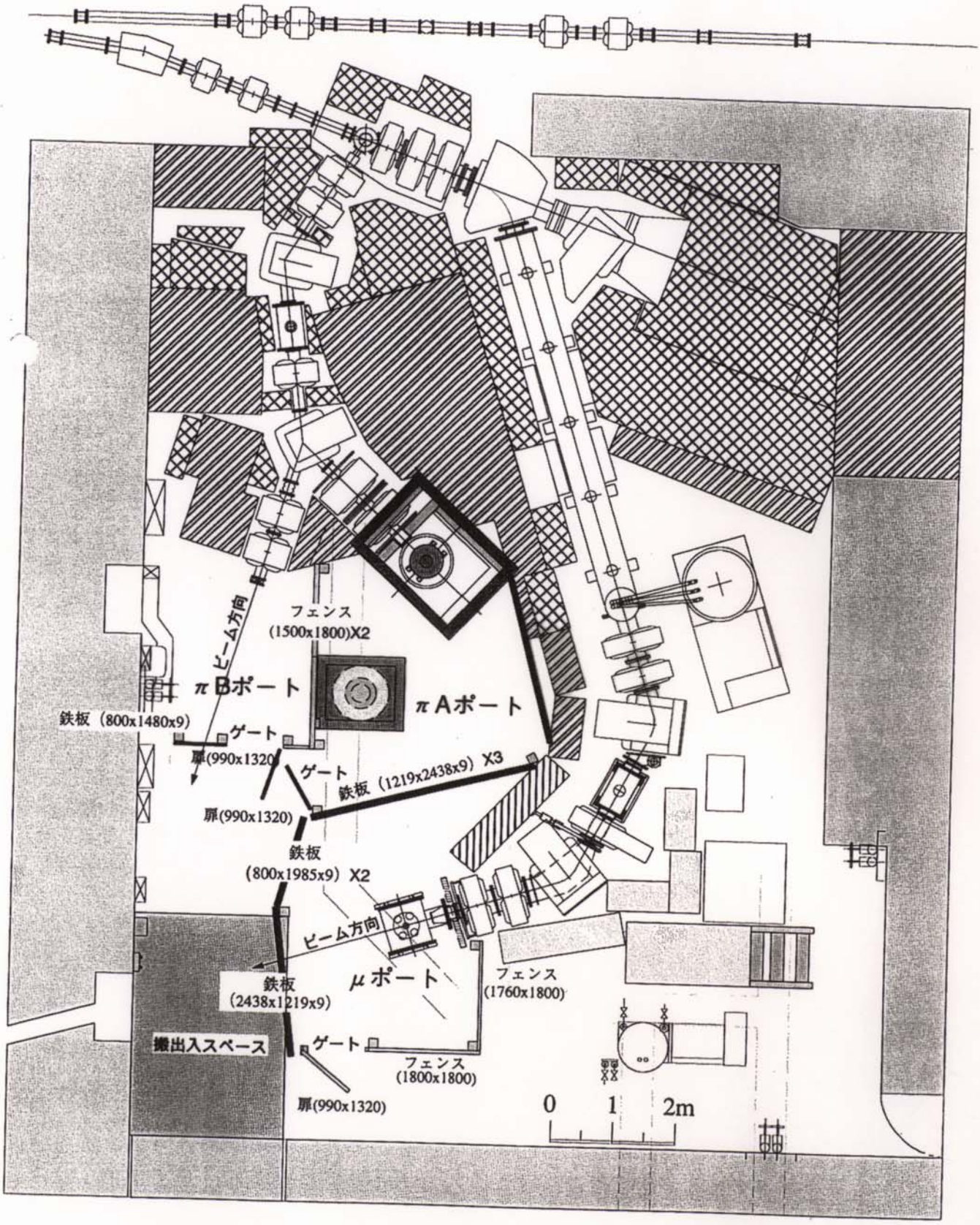

Implanted Muons in Matter

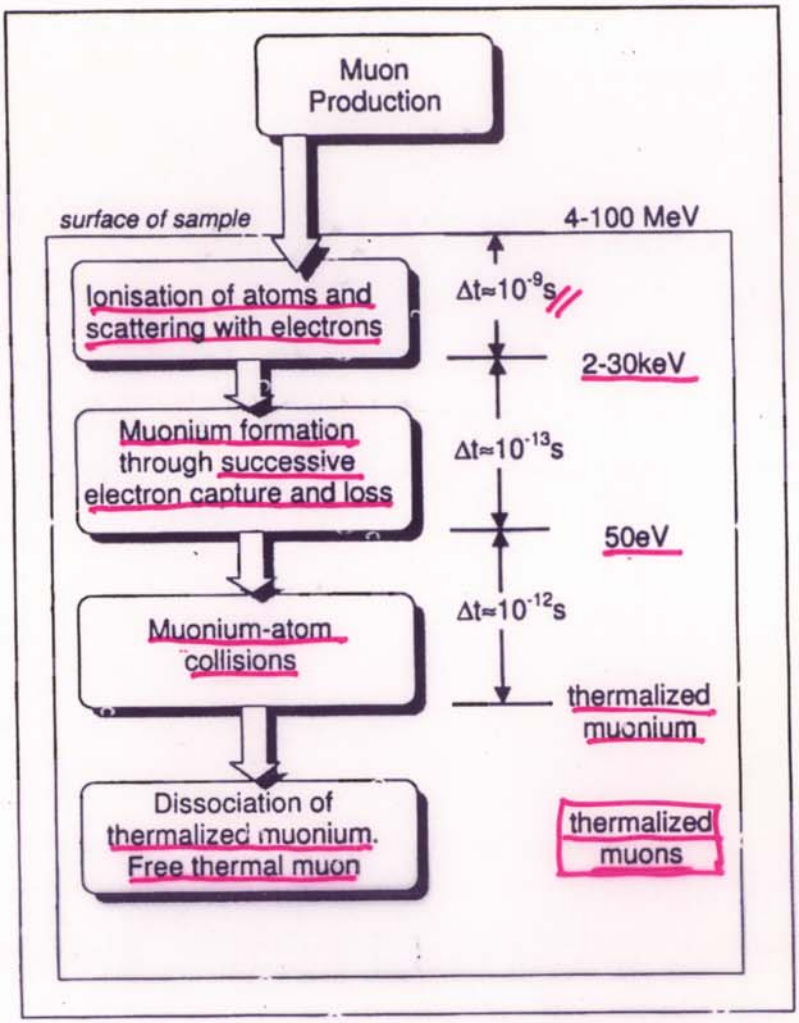

Figure 1. *Schematic representation of the processes of implantation and thermalisation of a muon within a sample. An indication of the time scales and muon energies at each stage of the process is provided. the final stage, that of the dissociation of thermal muonium, does not always occur, in which case it is the behaviour of the muonium atom within the sample that is studied.*

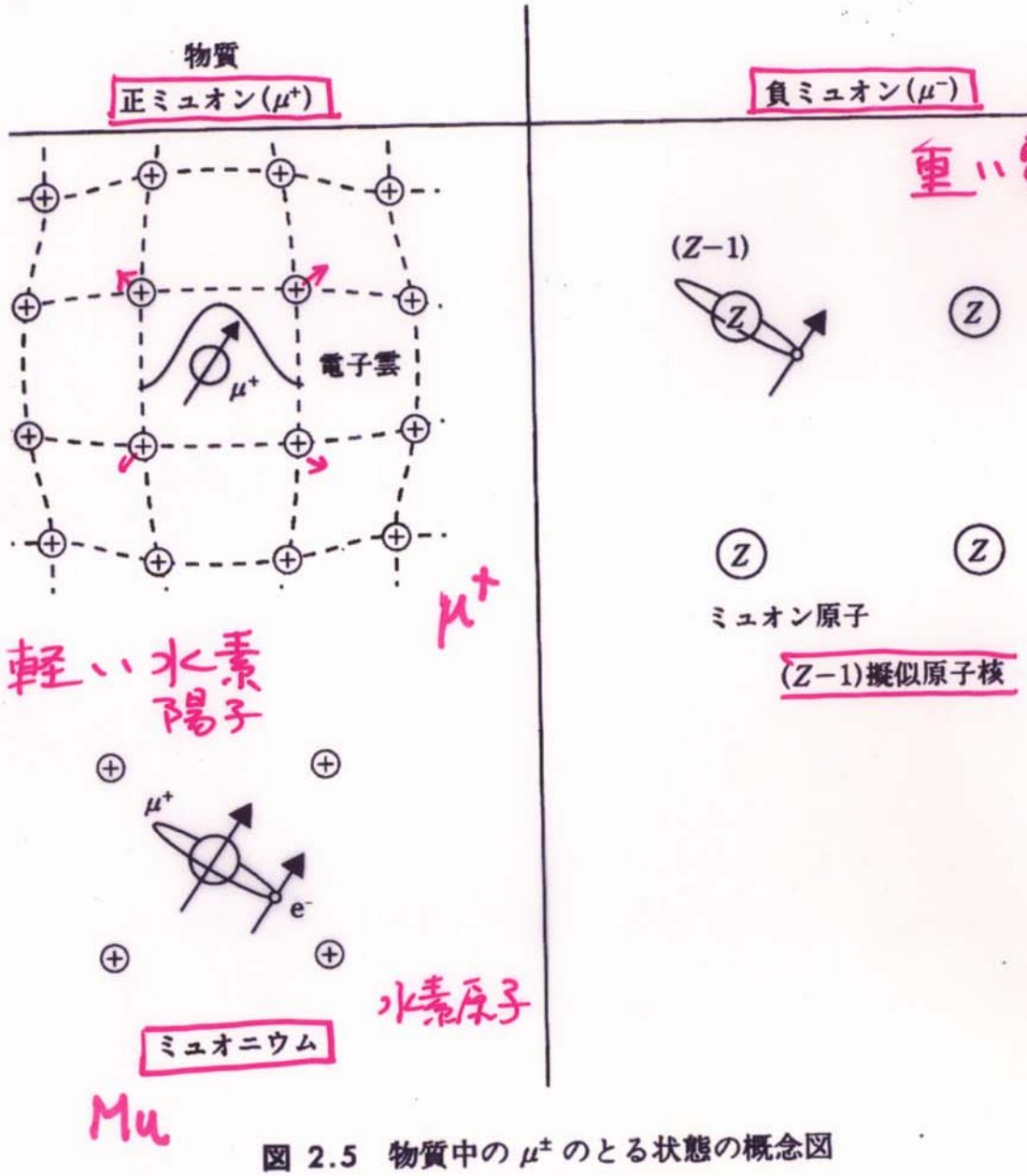

図 2.5　物質中の $\mu^{\pm}$ のとる状態の概念図

low H :

$$\frac{\gamma_{Mu}}{2\pi} \sim 13.9\ \mathrm{MHz/mT}$$

$$\frac{\gamma_{\mu^+}}{2\pi} \sim 135.554\ \mathrm{kHz/mT}$$

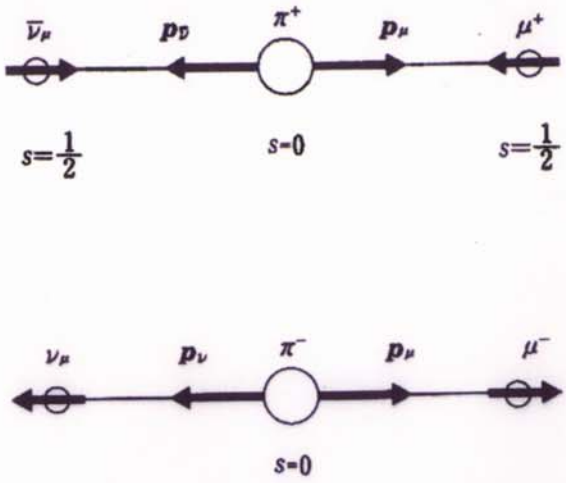

図 2.1　静止系におけるパイオンの崩壊

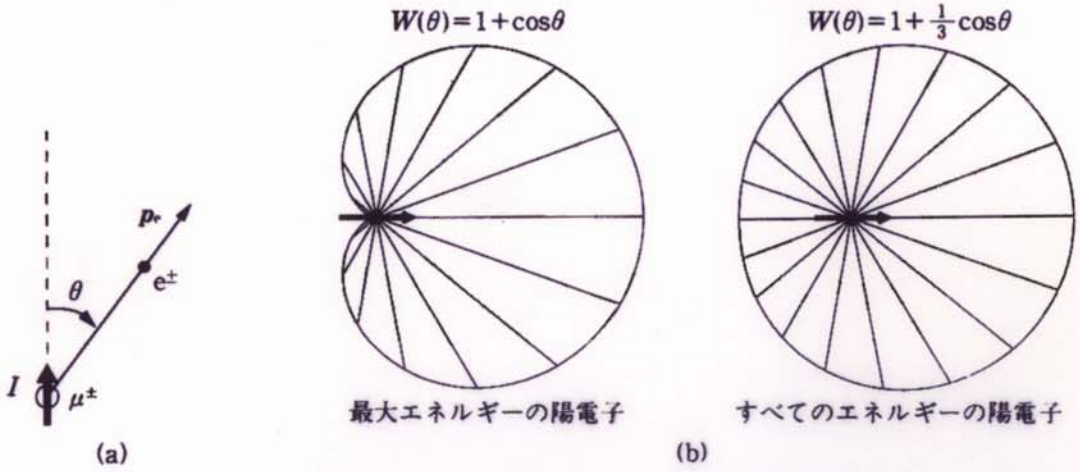

図 2.2　(a) ミュオン崩壊により放出される電子は，スピンの方向に対して空間異方性をもって放出される．(b) μ^+ の崩壊で放出される陽電子の角度分布．

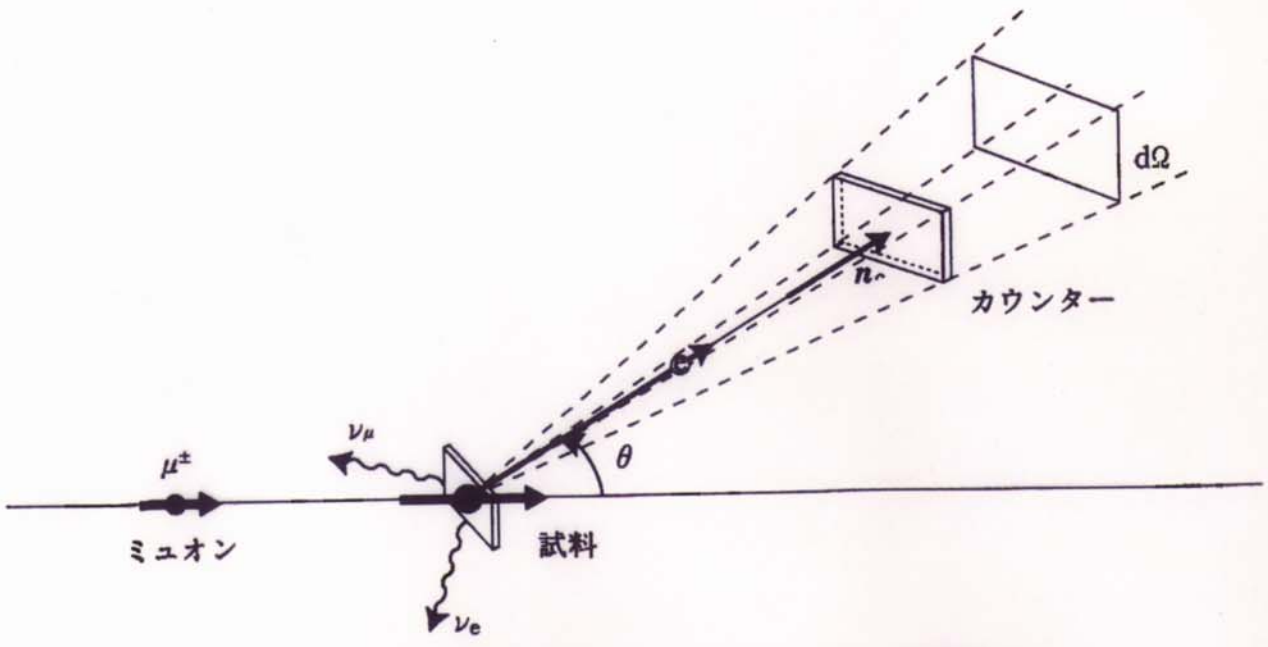

図 2.14　μSR 法によるミュオンスピン偏極測定

Quasiparticle spectra of high-temperature superconductors

B. L. Gyorffy
H H Wills Physics Laboratory, University of Bristol, Tyndall Avenue, Bristol, BS8 1TL, United Kingdom

Z. Szotek and W. M. Temmerman
Daresbury Laboratory, Warrington, WA4 4AD, United Kingdom

O. K. Andersen and O. Jepsen
Max-Planck-Institut für Festkörperforschung, Postfach 800665, D-70506, Stuttgart, Federal Republic of Germany

(Received 4 September 1997)

We present a semiphenomenological approach to calculating the quasiparticle spectra of high-temperature superconductors (HTSC's). It is based on a particularly efficient parametrization of the effective electron-electron interaction afforded by the density-functional theory for superconductors and a tight-binding linearized-muffin-tin-orbital scheme for solving the corresponding Kohn-Sham-Bogoliubov-de Gennes equations. We illustrate the method by investigating a number of site and orbital specific, but otherwise phenomenological, models of pairing in quantitative detail and discuss the results using BCS-like theory and insights to the HTSC band structures. We compare our results for the gap function on the Fermi surface with those deduced from photoemission experiments on single crystals of $YBa_2Cu_3O_7$. We also compare our predictions for the temperature dependence of the specific heat with measurements and conclude, provisionally, that the dominant pairing interaction operates between electrons of opposite spin, on nearest-neighbor Cu sites in $d_{x^2-y^2}$ orbitals. [S0163-1829(98)04426-9]

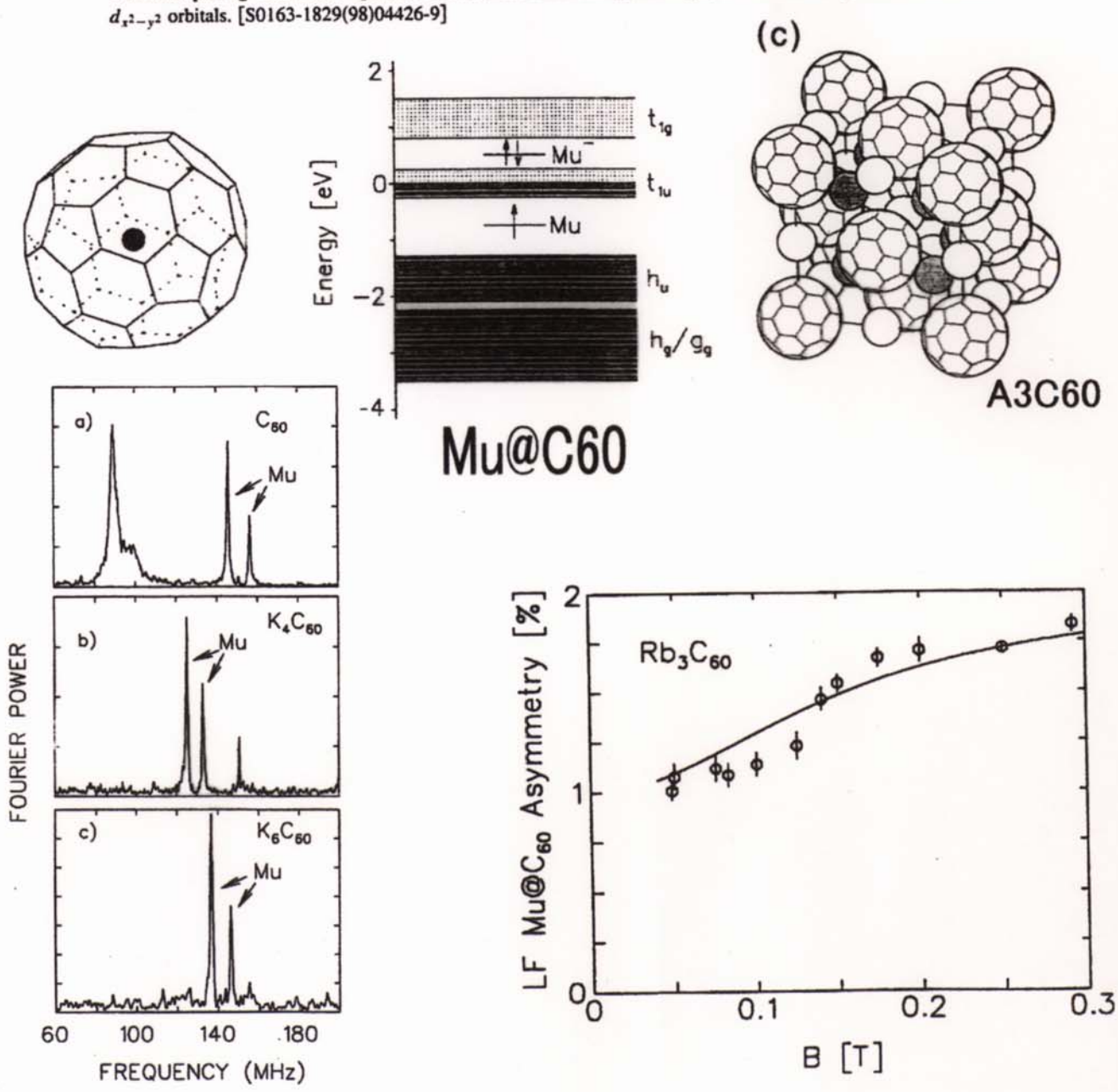

MSRの説明
TF-MSR と LF,ZF-MSR

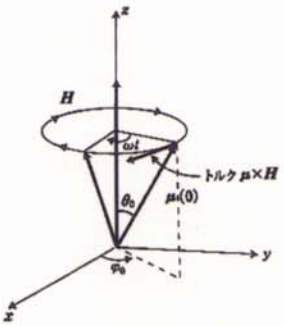

図 2.15 スピンのラーモア回転

TF-MSR

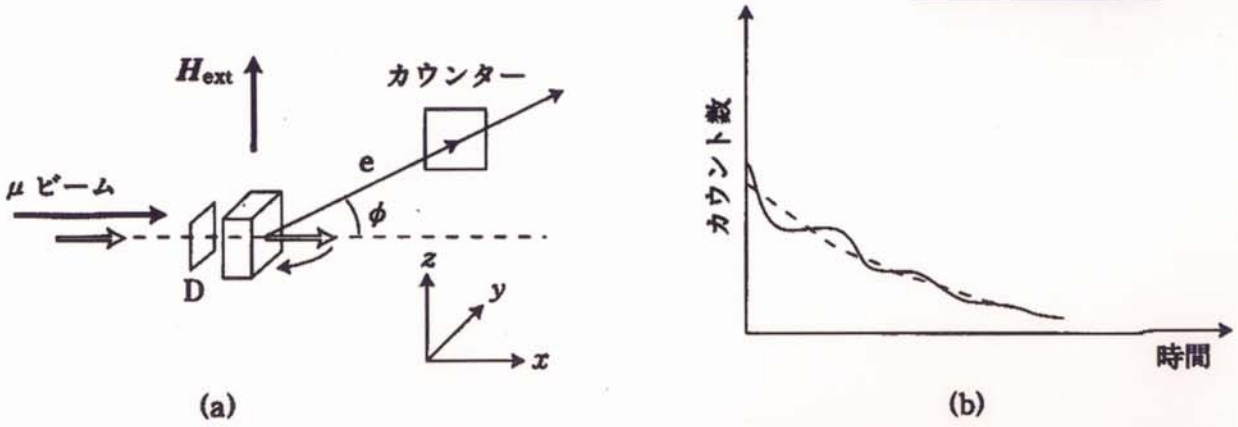

図 2.17 TF-μSR 法の概念図. (a) ミュオンスピン, 試料外部磁場, カウンターの配置. (b) カウンターで観測される μ-e 崩壊スペクトル.

LF-MSR

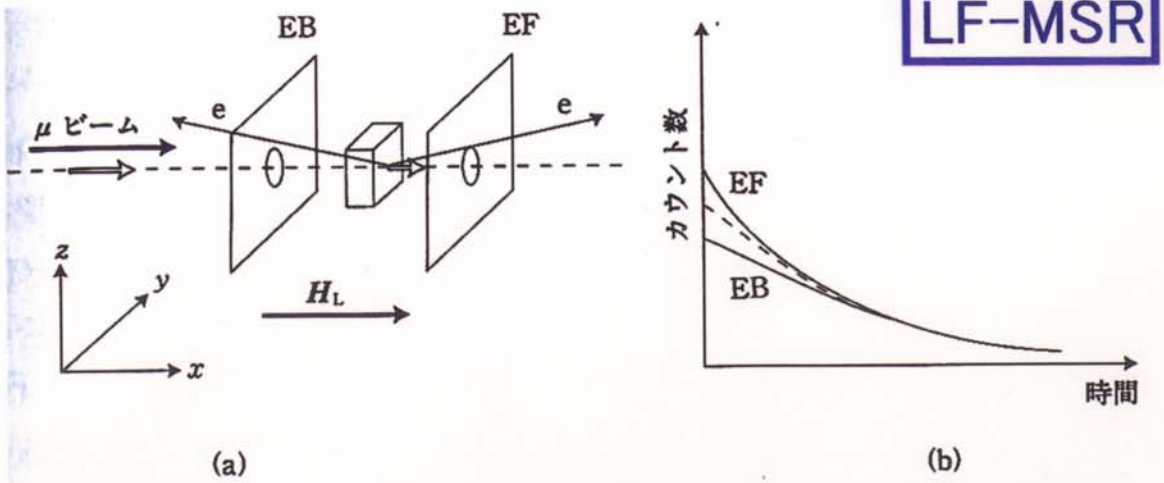

図 2.18 ZF-μSR, LF-μSR 法の概念図. (a) ミュオンスピン, 試料, 外部磁場, カウンターの配置. (b) カウンターで観測される μ-e 崩壊スペクトル.

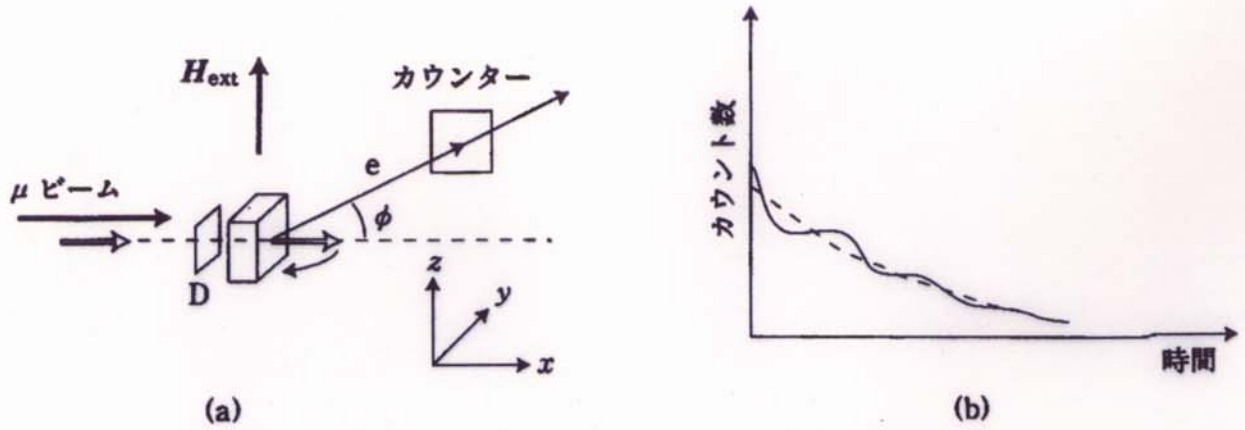

図 2.17　TF-μSR 法の概念図．(a) ミュオンスピン，試料外部磁場，カウンターの配置．(b) カウンターで観測される μ-e 崩壊スペクトル．

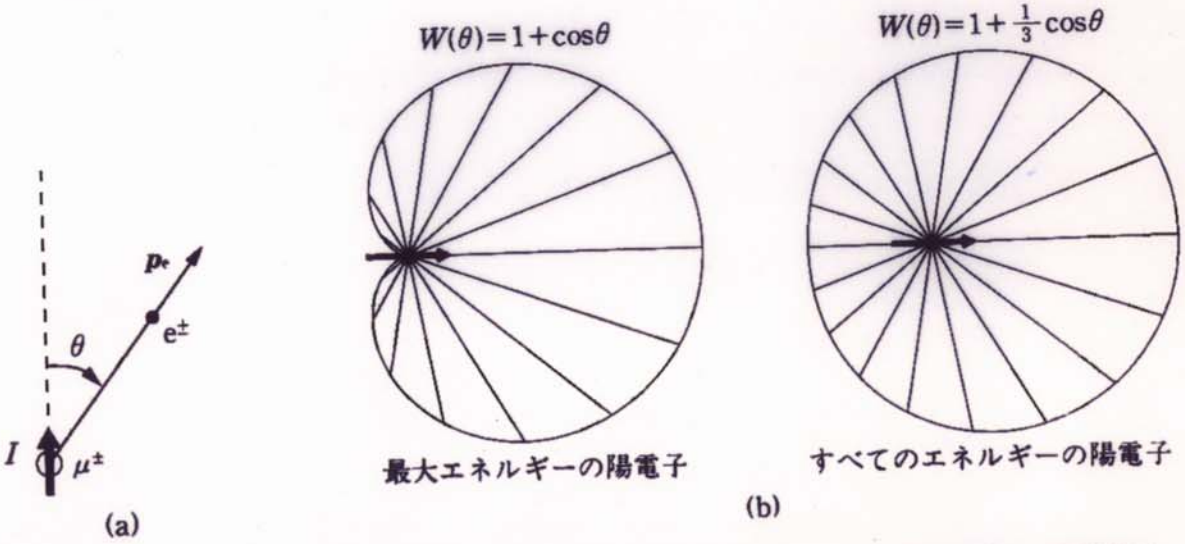

図 2.2　(a) ミュオン崩壊により放出される電子は，スピンの方向に対して空間異方性をもって放出される．(b) μ^+ の崩壊で放出される陽電子の角度分布．

表 2.1　ミュオンの基本的な性質

質　　量	$m_\mu = 105.65943(18)\,[\mathrm{MeV}/c^2]$ $= 0.1126096\,m_p$ $= 206.76855(36)\,m_e$
電　　荷	$+e(\mu^+)$,　　$-e(\mu^-)$
スピン(I)	1/2
磁気モーメント (μ_μ[erg/G])	$\mu_\mu = 4.49048\times10^{-23}$ $= 3.1833452(10)\,\mu_p$ $= 0.004836\,\mu_e$
g 因子 $\left(\mu_\mu = g\frac{e\hbar}{2m_\mu}I\right)$	$g_{\mu^+} = 2.002331820(24)$ $g_{\mu^-} = -2.002331872(24)$
磁気回転比 γ_μ (gyromagnetic ratio)	$\frac{\gamma_\mu}{2\pi} = 13.55342$ [kHz/G]
崩壊モード	$\mu^+ \longrightarrow e^+ + \nu_e + \overline{\nu_\mu}$ $\mu^- \longrightarrow e^- + \overline{\nu_e} + \nu_\mu$
寿　命 (τ_μ)	2.19714(7) [μs]

表 2.3　μ^+SR と μ^-SR との比較

	μ^+SR	μ^-SR
位　　置	格子間隔	格子位置
大 き さ	零点振動振幅	$\frac{2.55}{Z}\times10^{-11}$ cm
プローブ	水素の同位体	マイナス　($Z-1$)不純物
寿　　命	2.2 μs	0.08～2 μs
g 因 子	g_{free}^+	$\left[1-\frac{1}{3}(aZ)^2\right]\times g_{free}^-$
偏 極 度	100%	～16%

表 2.2　ミュオニウム Mu(μ^+e^-) の基底状態の性質(真空中)

ボーア半径 a_B	$1.004\,a_H$
イオン化エネルギー I	$0.996\,I_H$
超微細結合定数 A	$4463\,\mathrm{MHz} \cong \left(\frac{\mu_\mu}{\mu_p}\right)A_H$
四重極モーメント*) $Q_{Mu}(F=1)$	$-\frac{\mu_{\mu^+}\mu_e}{3m_\mu} \sim -2.0\times10^{-24}\,\mathrm{cm}^2$

*)　真空中のミュオニウムの $1s_{1/2}$ の 3 重項状態 ($F=1$) においては，μ^+ と e^- の磁気双極子・磁気双極子相互作用により，3d 状態が混じり，小さな四重極モーメントをもつことが計算から示されるが実験的には検証されていない．

表 2.3　ミュオン原子

大 き さ	$\frac{2.55}{Z}\times10^{-11}$ [cm]	
寿　　命	$\sim 2\,\mu$s	$Z<7$
	$\sim\frac{1}{200Z^4}$	$7<Z<40$
	0.08 μs	$Z>40$
g 因 子	$\left[1-\frac{1}{3}(aZ)^2\cdots\cdots\right]\times g_{free}$	

$$r_{1s} = \frac{1}{Z}a_B^{\mu}$$

$$= \frac{1}{Z}\frac{m_e}{m_\mu}a_B^{e}$$

$$= \frac{1}{Z}\times 2.55\times10^{-11}\,[\mathrm{cm}]$$

$$\Psi_{1s}(r) = \left(\frac{1}{\pi}\right)^{1/2}\left(\frac{1}{r_{1s}}\right)^{3/2}\exp\left(-\frac{r}{r_{1s}}\right) = \left(\frac{1}{\pi}\right)^{1/2}\left(\frac{Z}{a_B^{\mu}}\right)^{3/2}\exp\left(-\frac{Zr}{a_B^{\mu}}\right)$$

$$E_n = -\frac{1}{n^2}\frac{m^{\mu}}{m_e}Z\times13.6\,[\mathrm{eV}]$$

$$= -\frac{Z}{n^2}\times2.82\,[\mathrm{keV}]$$

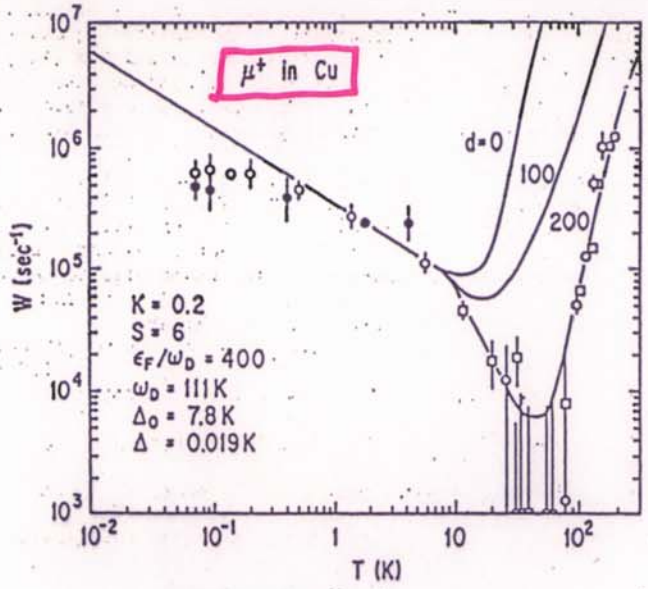

Fig. 3 The hopping rate of the positive muon in Cu. The best fit to the experiment /10/ is obtained for d(quadratic coupling constant)=200.

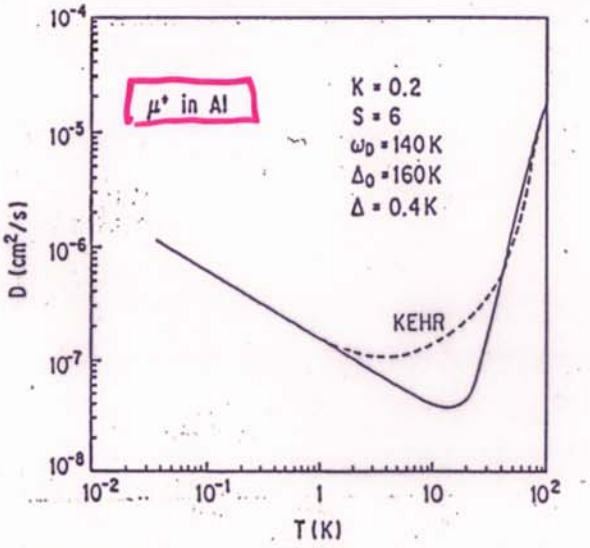

Fig. 4 The hopping rate of the positive muon in Al. The fit to the experiment /5/ is good except the temperature region around 10K.

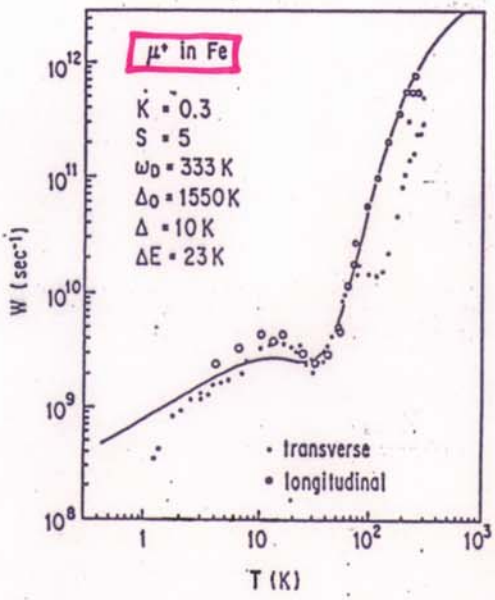

Fig. 5 The hopping rate of the positive muon in Fe. Longitudinal data are for the external field of 2.0T. The maximum around 10K is obtained theoretically only by assuming a large inhomogeneous broadening ΔE.

Quantum Diffusion of positive muon in metals

μ^+ site in MgB_2

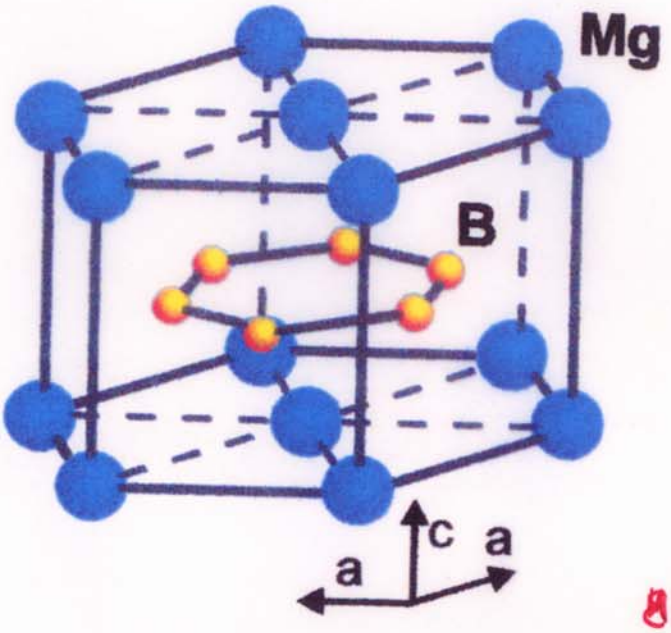

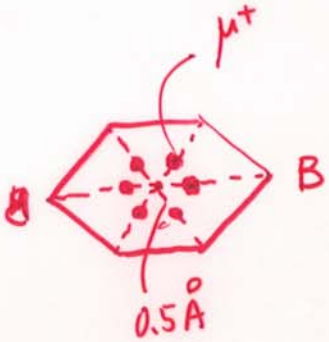

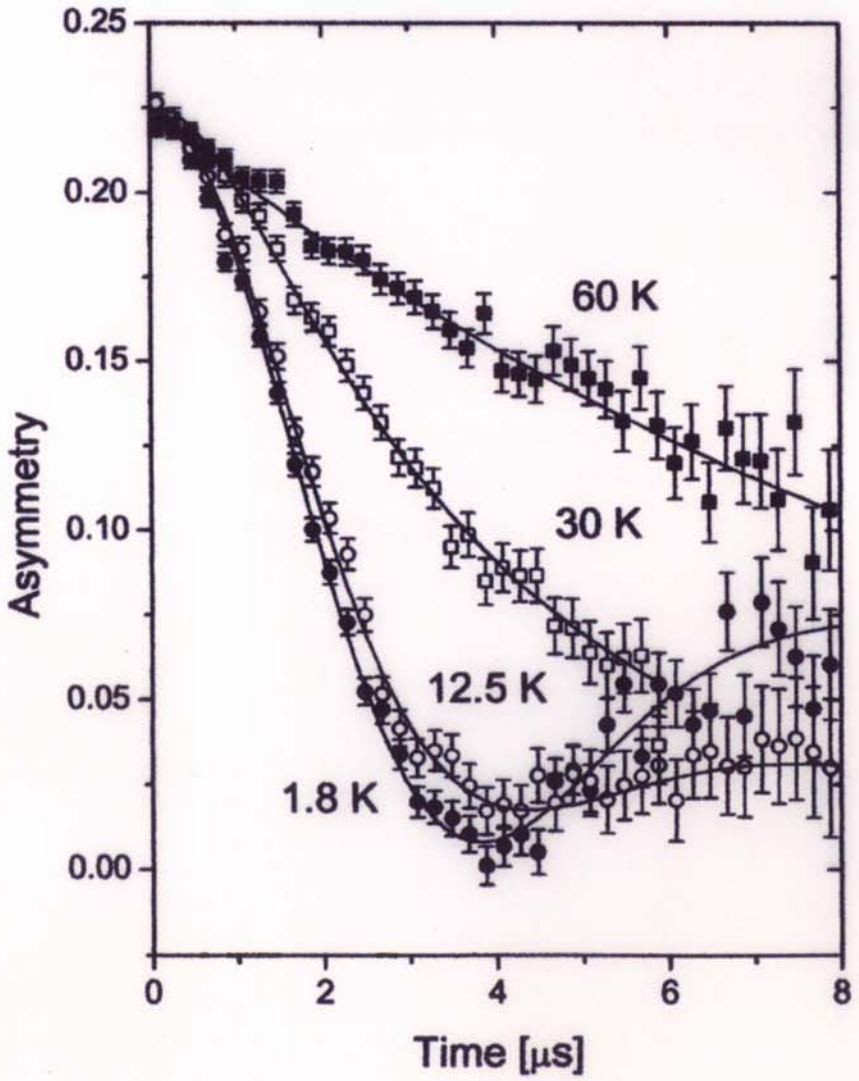

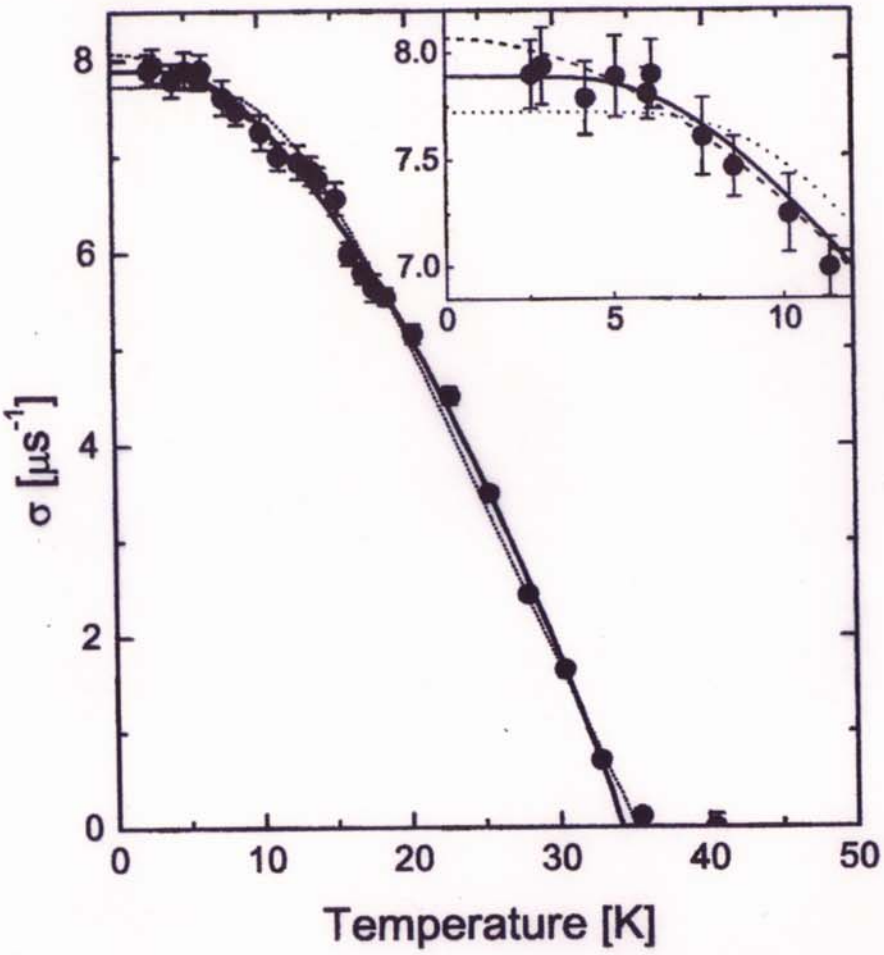

Two-band theory

Δ_L =6.0meV
$2\Delta/kT_c$ =3.6
Δ_S =2.6meV
$2\Delta/kT_c$ =1.6

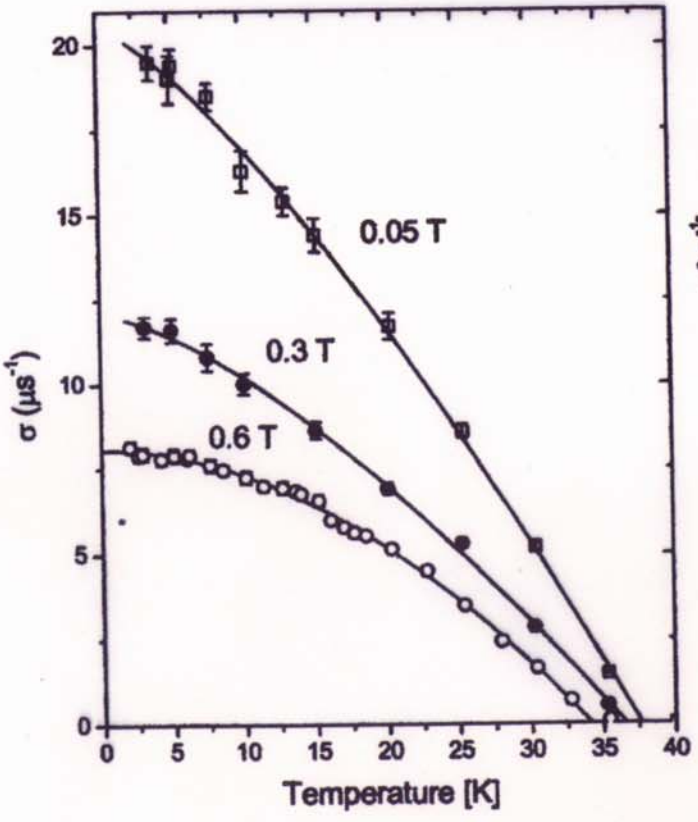

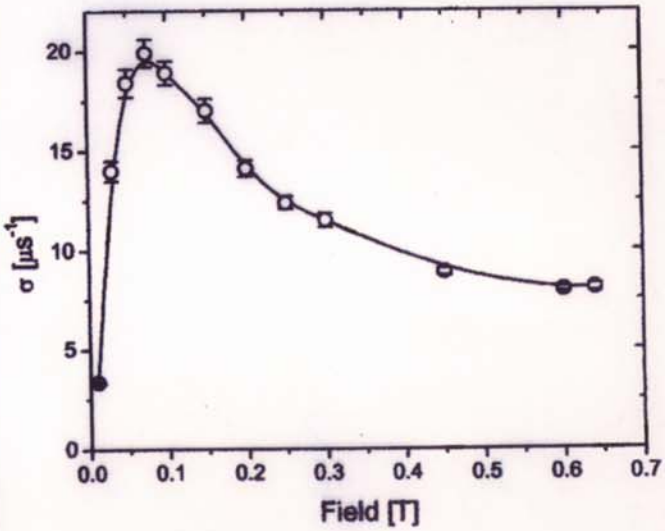

Niedermeyer et al (2001)

R. Feyerherm et al. PRL 73 (1994) 1849, Physica B194-196 (1994) 357

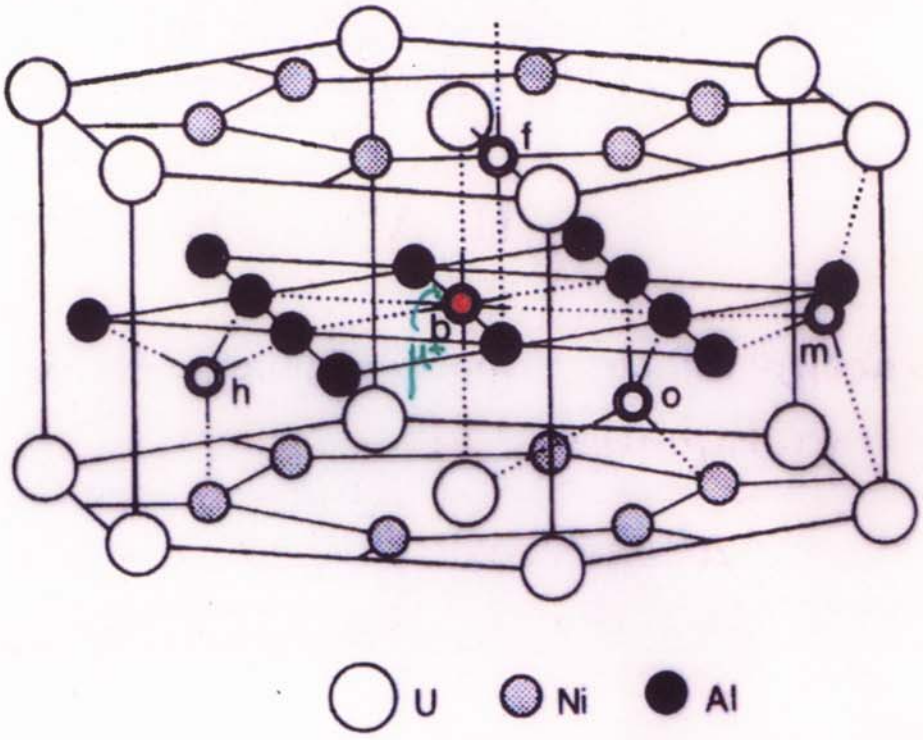

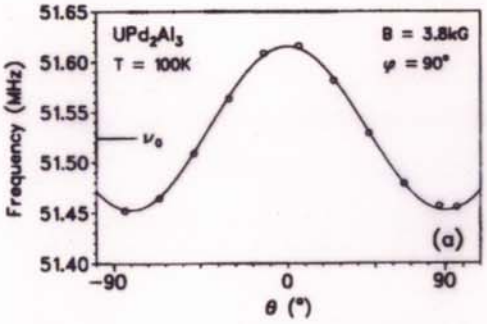

Figure 2.4. *Measured angular dependence of K in UPd_2Al_3, rotating H_{ext} in the $(b^* - c)$ plane. (Feyerherm, 1995; see also Amato, 1997).*

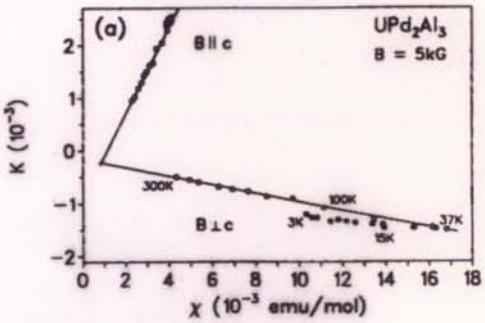

Figure 2.5. *Knight shift versus susceptibility for $H_{ext} \| c$-axis and $H_{ext} \perp c$-axis (Feyerherm 1995).*

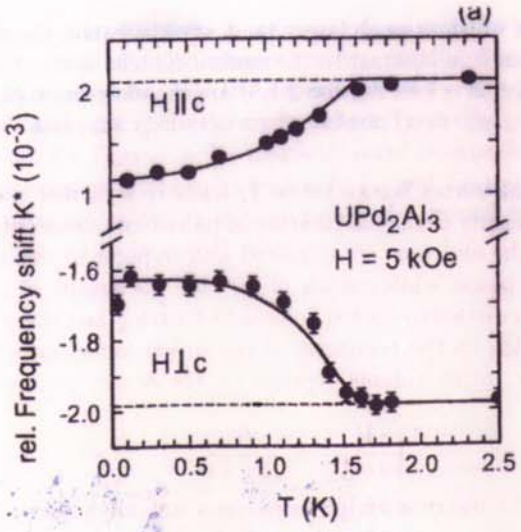

Muon Spin resonance

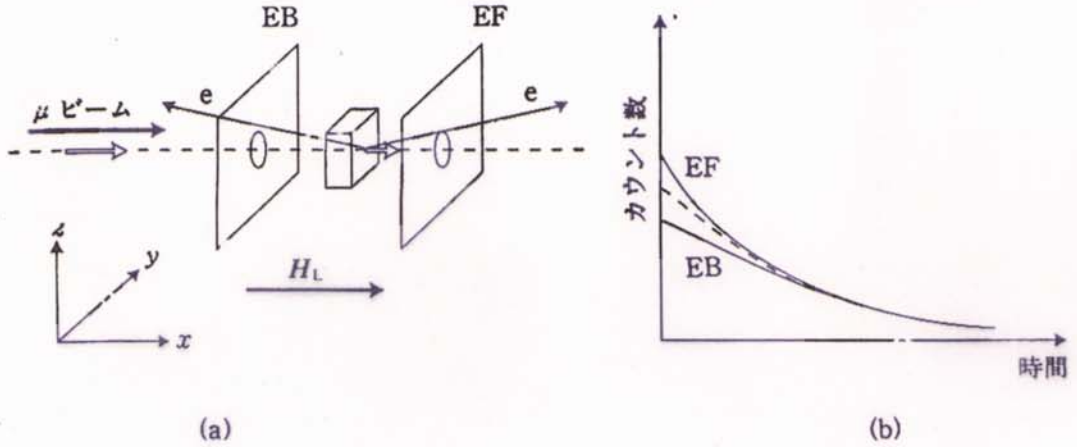

図 2 18 ZF-μSR, LF-μSR 法の概念図. (a) ミュオンスピン, 試料, 外部磁場, カウンターの配置. (b) カウンターで観測される μ-e 崩壊スペクトル.

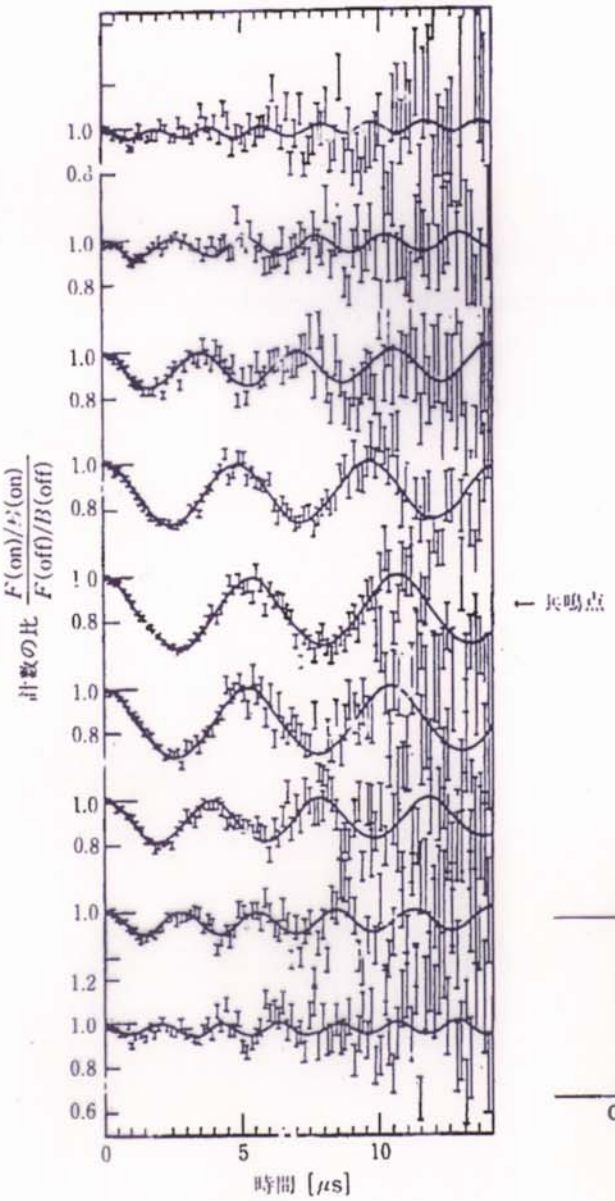

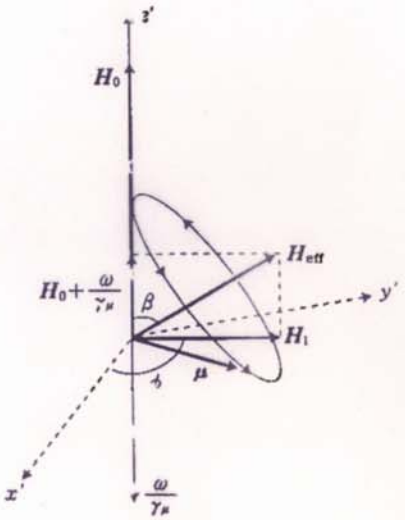

図 2.40 回転座標系における外部磁場と高周波磁場

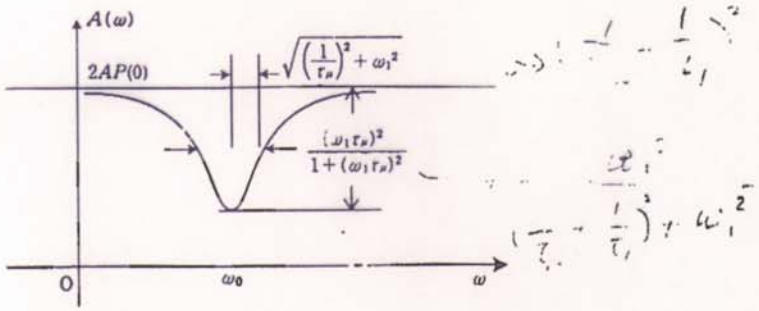

図 2.42 共鳴曲線

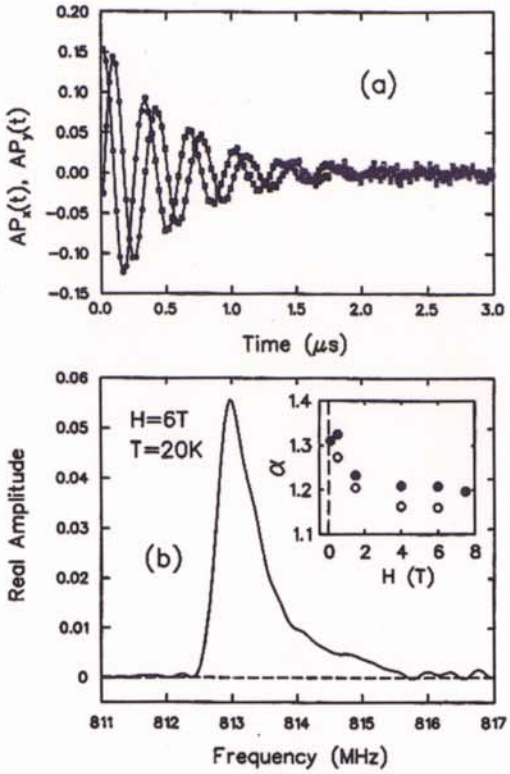

FIG. 1. (a) The muon spin precession signal at $T = 20$ K and $H = 6.0$ T displayed in a reference frame rotating at about 3 MHz below the Larmor precession frequency of a free muon in the external field (note: a is the maximum precession amplitude). (b) The FFT of (a) using a Gaussian apodization with a 3 μs time constant. Inset: Field dependence of the skewness parameter α extrapolated to $T = 0$ K (solid circles) and at $T = 50$ K (open circles).

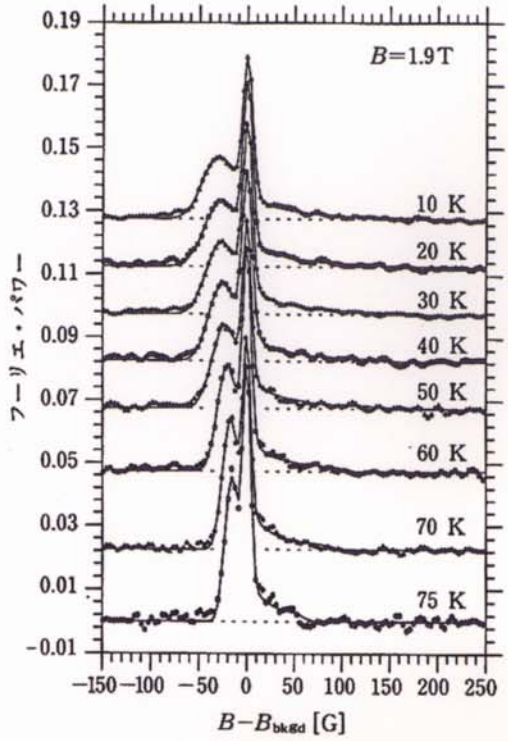

図 2.32 $YBa_2Cu_3O_7$ の TF-μ^+SR のフーリエ・スペクトル[34]

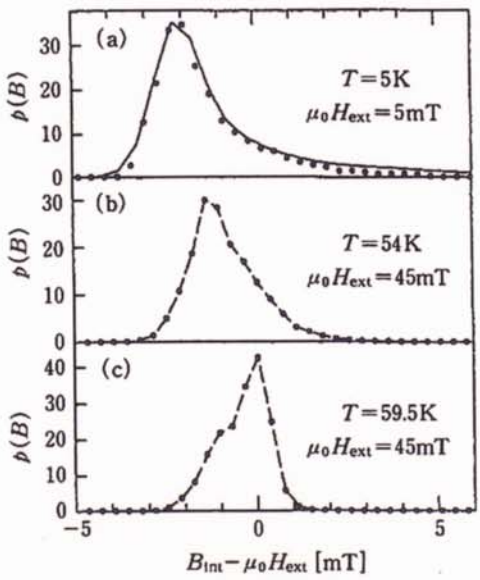

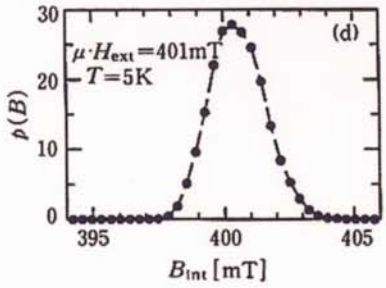

図 2.33 $Bi_2Sr_2CaCu_2O_x$ の TF-μ^+SR[35]

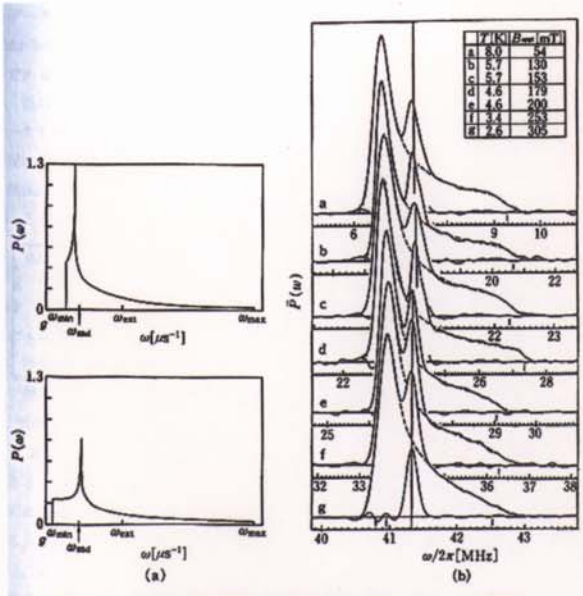

図 2.31 Nb 中の TF-μ^+SR. (a) 第2種超伝導体の磁場分布(計算値). (b) 磁場中の Nb の μ^+SR による磁場分布測定[33].

$YBa_2Cu_3O_x$

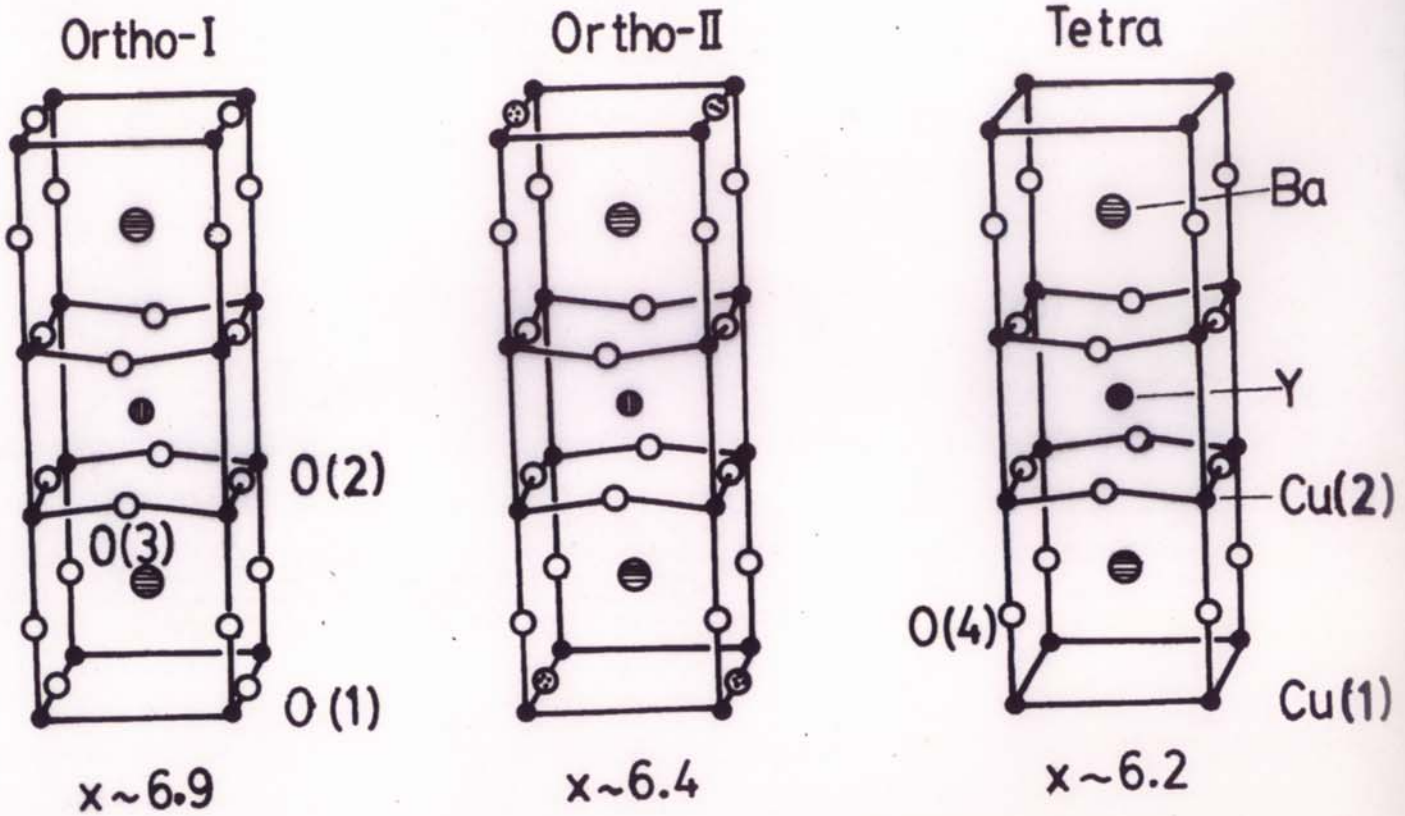
Ortho-I
Ortho-II
Tetra
O(2)
O(3)
O(1)
Ba
Y
Cu(2)
O(4)
Cu(1)
x~6.9
x~6.4
x~6.2

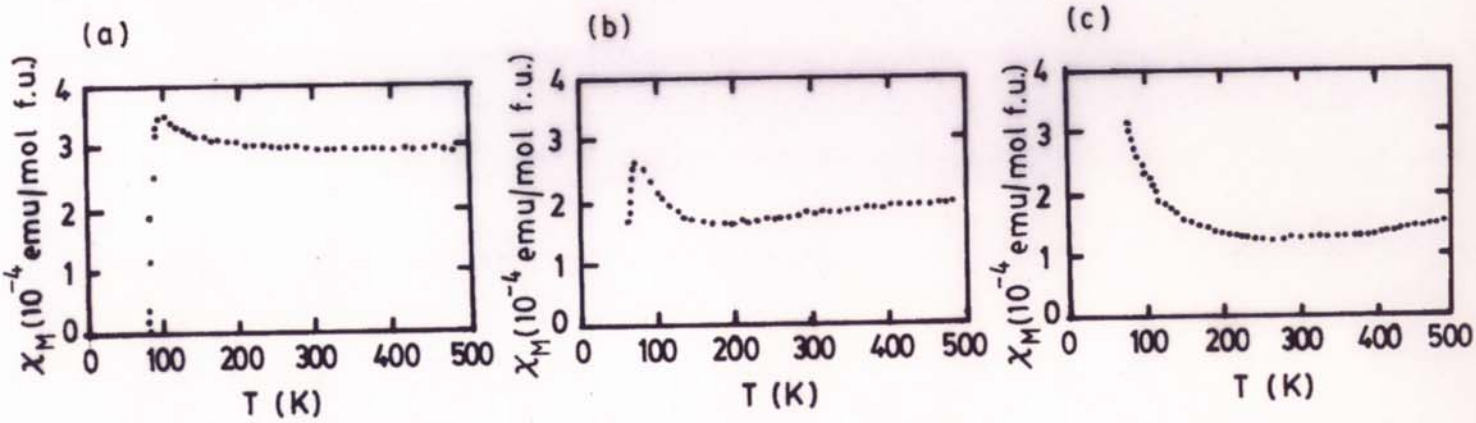
(a)
(b)
(c)
$\chi_M(10^{-4}$ emu/mol f.u.)
T (K)

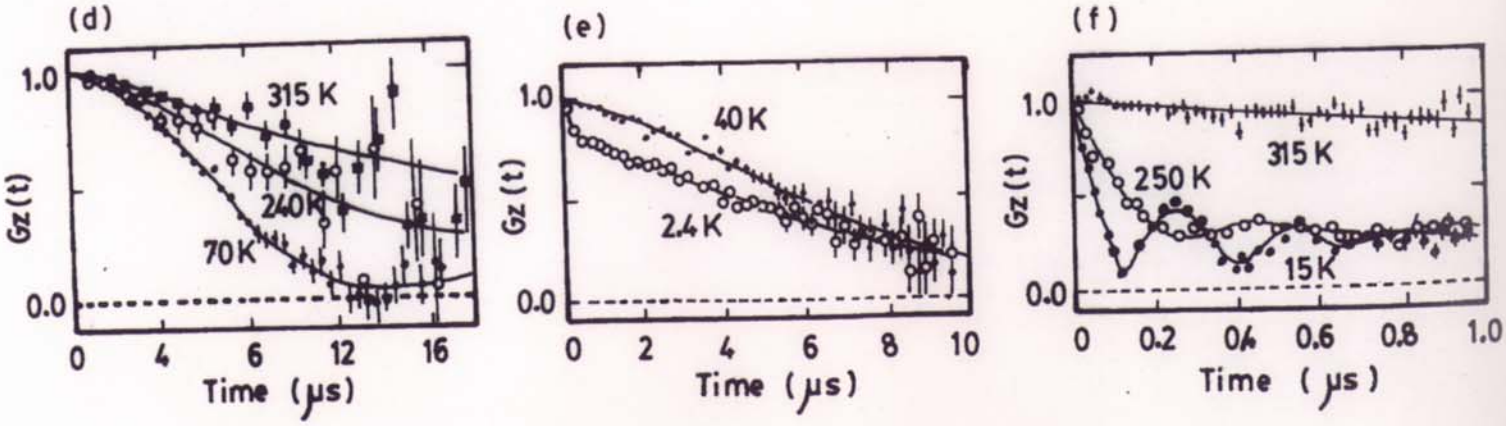
(d)
(e)
(f)
Gz(t)
315 K
240K
70K
40K
2.4K
250 K
15K
Time (μs)

oxygen-ordering in Cu(1)O plane
separation into micrograins of insulating (oxygen-disorder) phase and superconducting (oxygen-ordered) phase
~50Å

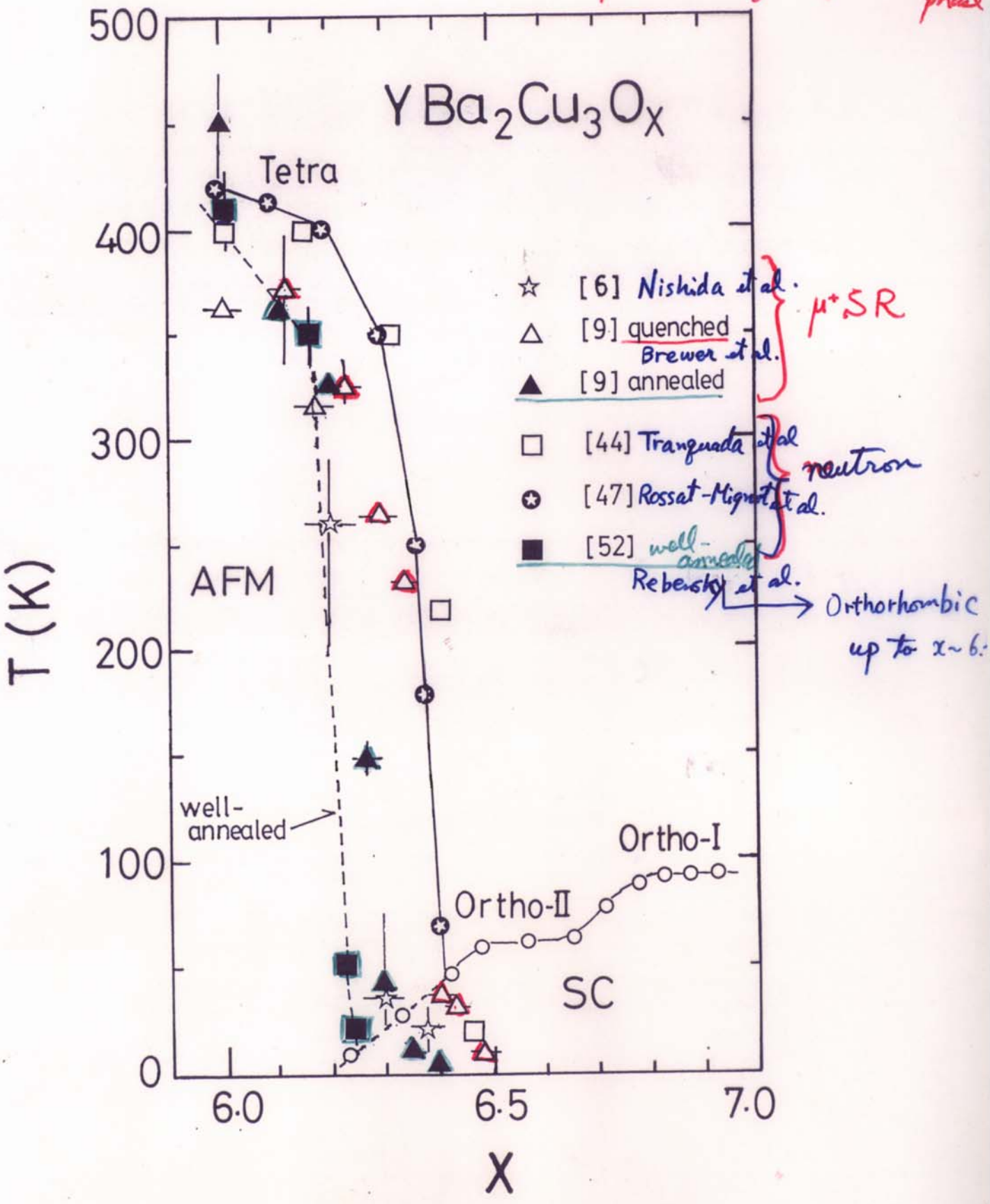

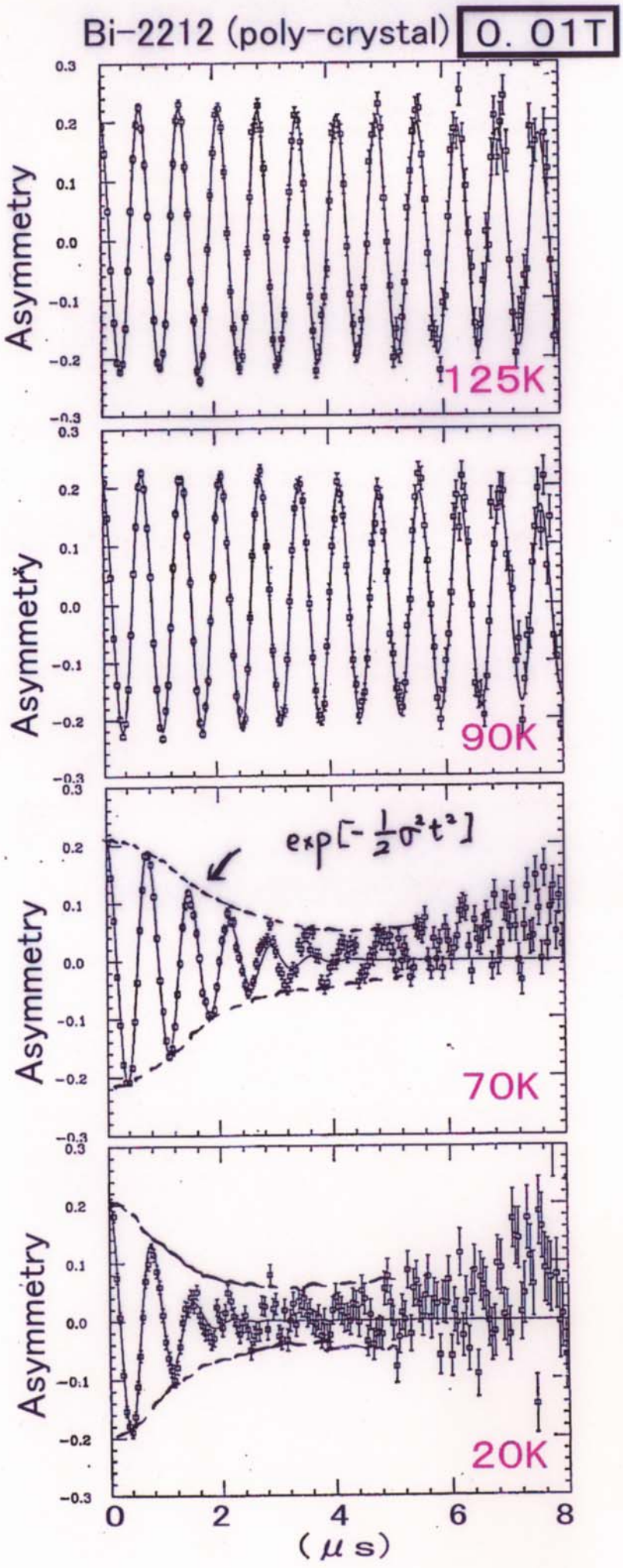

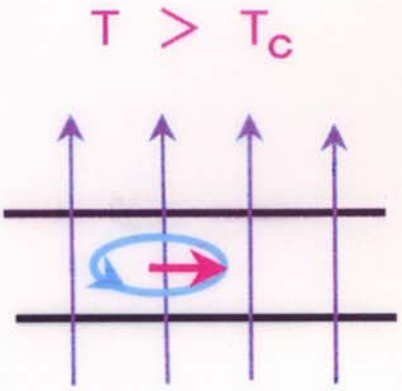

$$\sigma \propto \sqrt{\Delta B^2}$$

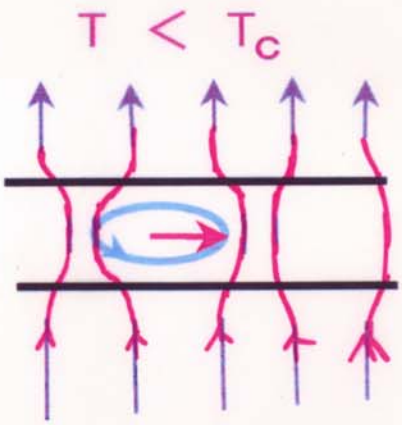

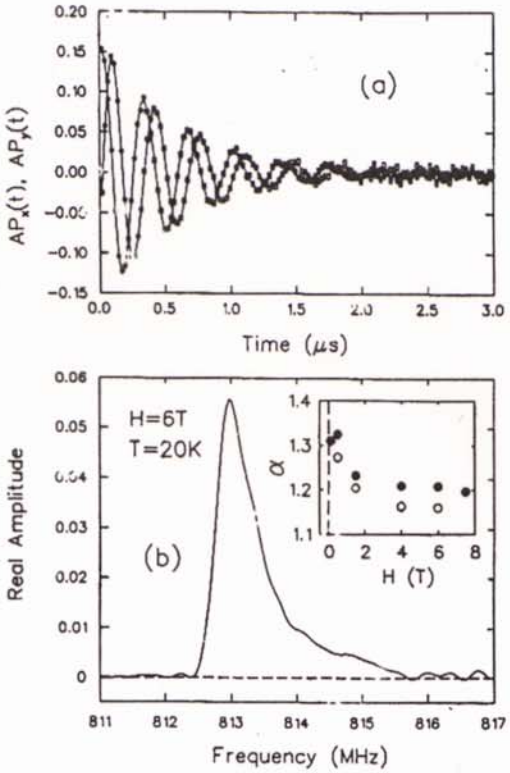

FIG. 1. (a) The muon spin precession signal at $T = 20$ K and $H = 6.0$ T displayed in a reference frame rotating at about 3 MHz below the Larmor precession frequency of a free muon in the external field (note: a is the maximum precession amplitude). (b) The FFT of (a) using a Gaussian apodization with a 3 μs time constant. Inset: Field dependence of the skewness parameter α extrapolated to $T = 0$ K (solid circles) and at $T = 50$ K (open circles).

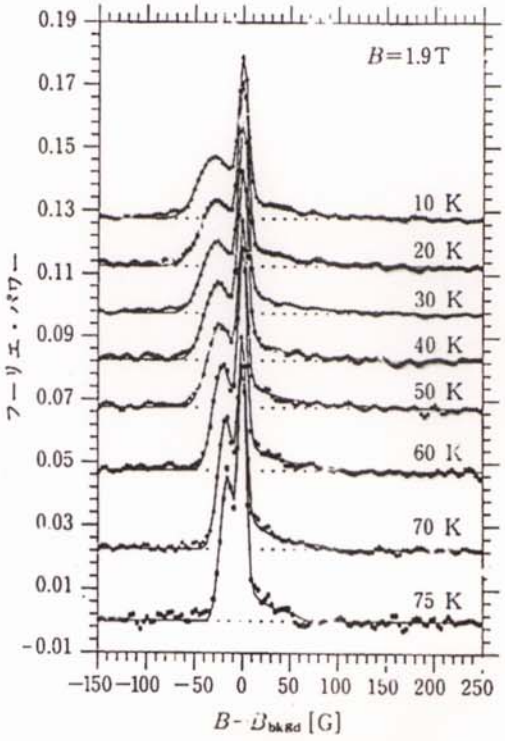

図 2.32 $YBa_2Cu_3O_7$ の TF-μ^+SR のフーリエ・スペクトル[34]

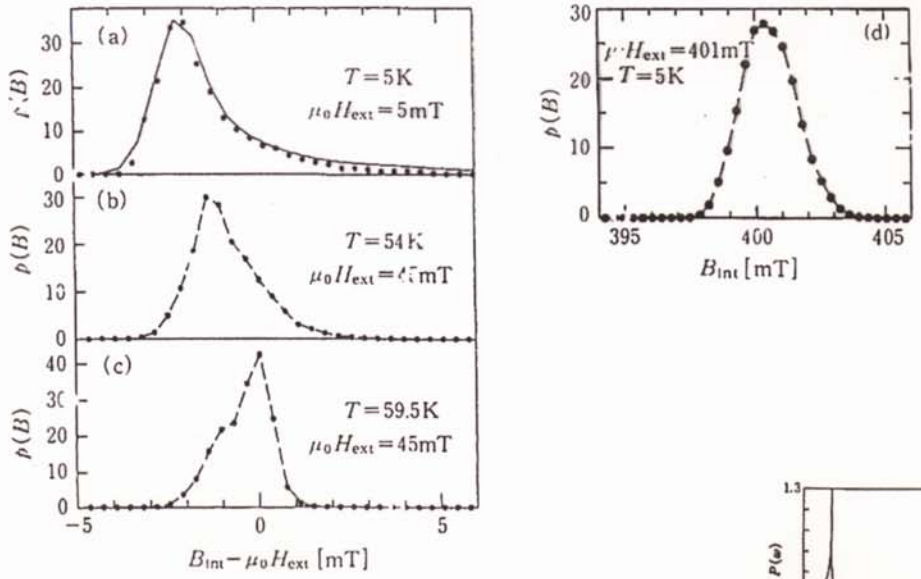

図 2.33 $Bi_2Sr_2CaCu_2O_x$ の TF-μ^+SR[35]

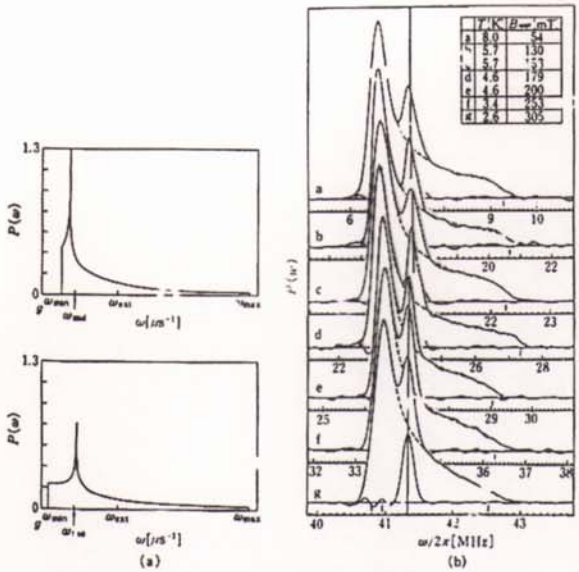

図 2.31 Nb 中の TF-μ^+SR. (a) 第2種超伝導体の磁場分布(計算値). (b) 磁場中の Nb の μ^+SR による磁場分布測定[33].

$Pb_{0.9}\,In_{0.1}$

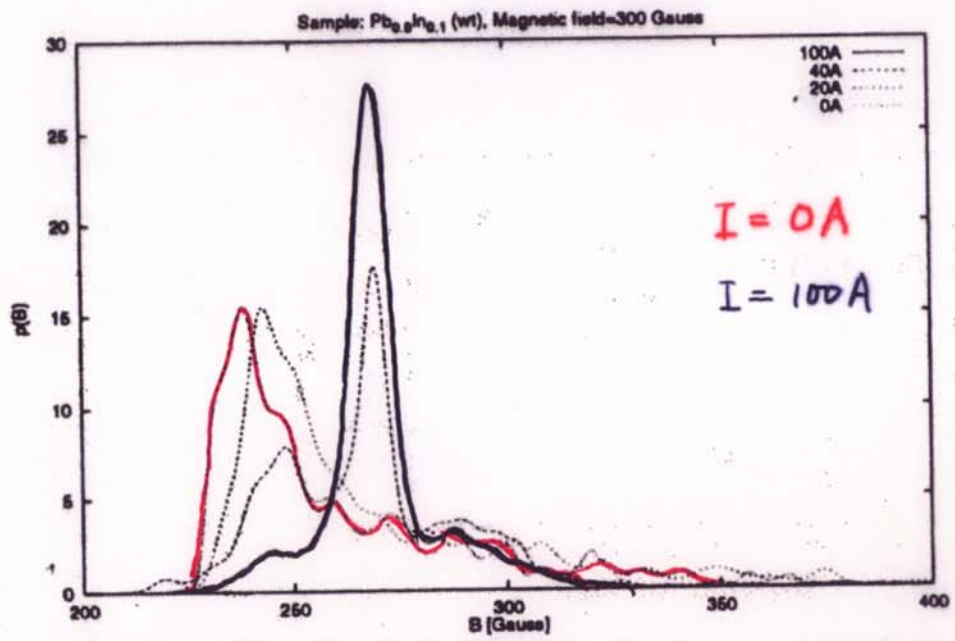

Figure 1: The effect of a transport current on the $p(B)$ lineshape (background at applied field subtracted).

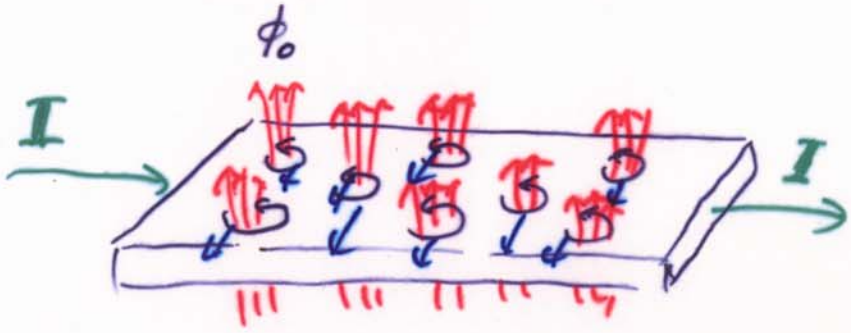

E.M. Forgan et al. : RB 11358 (2000)
Rutherford Report

Field Induced Reduction of the Low-Temperature Superfluid Density in $YBa_2Cu_3O_{6.95}$

J. E. Sonier,[1,2] J. H. Brewer,[2,3] R. F. Kiefl,[2,3] G. D. Morris,[2] R. I. Miller,[2,3] D. A. Bonn,[3]
J. Chakhalian,[2,3] R. H. Heffner,[1,2] W. N. Hardy,[3] and R. Liang[3]
[1]*Los Alamos National Laboratory, Los Alamos, New Mexico 87545*
[2]*TRIUMF, Vancouver, British Columbia, Canada V6T 2A3*
[3]*Department of Physics and Astronomy, University of British Columbia, Vancouver, British Columbia, Canada V6T 1Z1*
(Received 30 June 1999)

A novel high magnetic field (8 T) spectrometer for muon spin rotation has been used to measure the temperature dependence of the in-plane magnetic penetration depth λ_{ab} in $YBa_2Cu_3O_{6.95}$. At low H and low T, λ_{ab} exhibits the characteristic linear T dependence associated with the energy gap of a $d_{x^2-y^2}$-wave superconductor. However, at higher fields λ_{ab} is essentially temperature independent at low T. We discuss possible interpretations of this surprising new feature in the low-energy excitation spectrum.

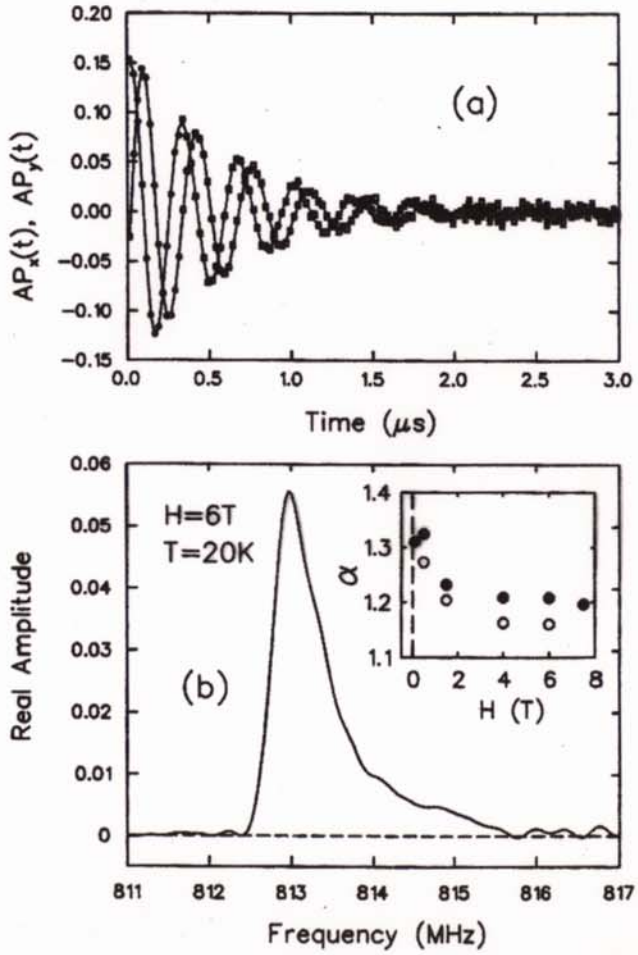

FIG. 1. (a) The muon spin precession signal at $T = 20$ K and $H = 6.0$ T displayed in a reference frame rotating at about 3 MHz below the Larmor precession frequency of a free muon in the external field (note: a is the maximum precession amplitude). (b) The FFT of (a) using a Gaussian apodization with a 3 μs time constant. Inset: Field dependence of the skewness parameter α extrapolated to $T = 0$ K (solid circles) and at $T = 50$ K (open circles).

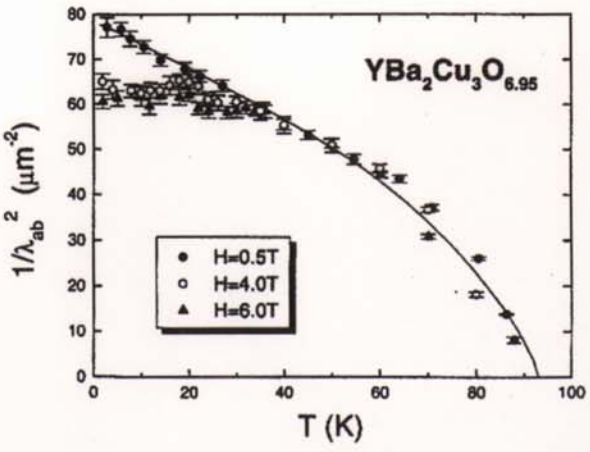

FIG. 2. Temperature dependence of λ_{ab}^{-2} at $H = 0.5$, 4, and 6 T. The solid curve represents the zero-field microwave measurements of $\Delta\lambda_{ab}(T)$ in Ref. [1].

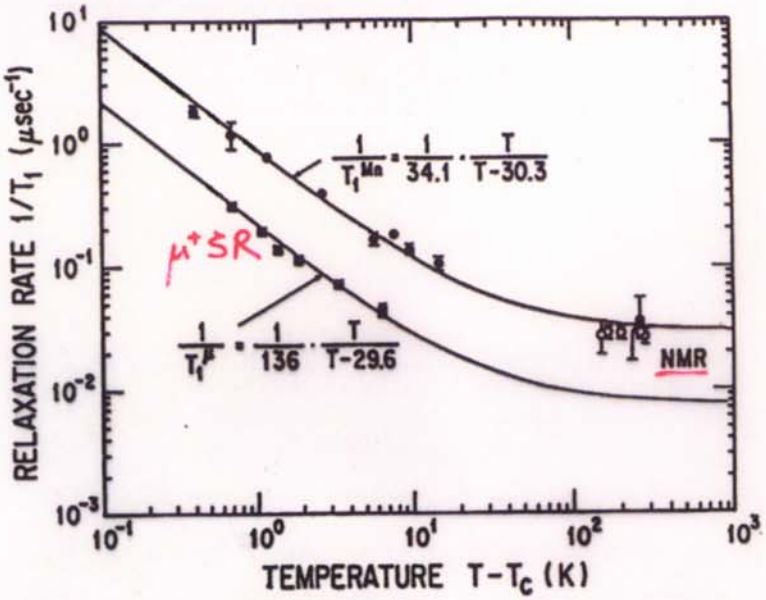

SCR - Theory
(Moriya)

Figure 3. The ^{55}Mn nuclear spin relaxation rate ($1/T_1^{Mn}$, closed circles) and μ^+ spin relaxation rate ($1/T_1^{\mu}$, closed squares) in MnSi obtained in the present ZF-μ^+SR experiment are plotted against $T - T_c$. The solid curve shows the best-fitted theoretical relaxation rate by assuming the Moriya expression Eq.(2). Also shown are the ^{55}Mn NMR data (open circles, Ref.2) for comparison.

T. Matsuzaki, K. Nishiyama, K. Nagamine, T. Yamazaki et al. Phys. Lett. A123 (1987) 92.

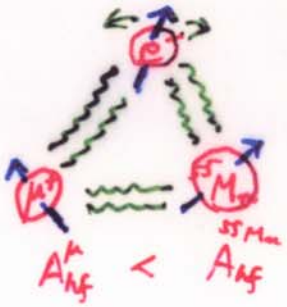

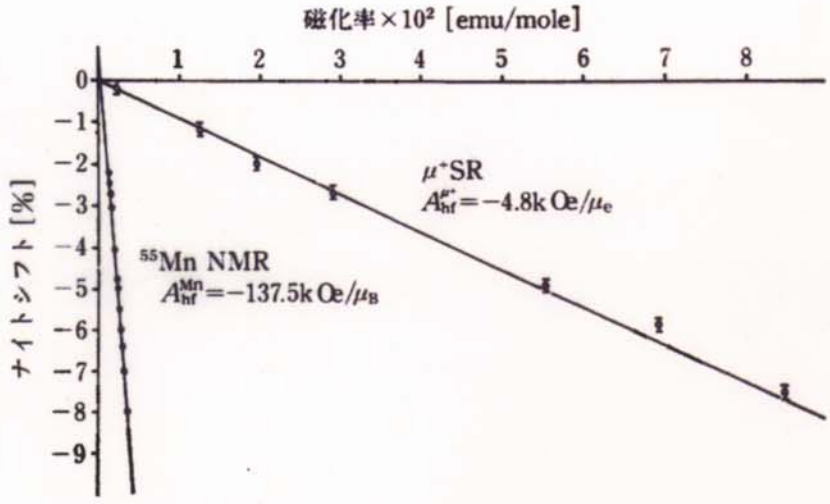

図 2.37 MnSi の μ^+, ^{55}Mn の K-χ プロット[43]

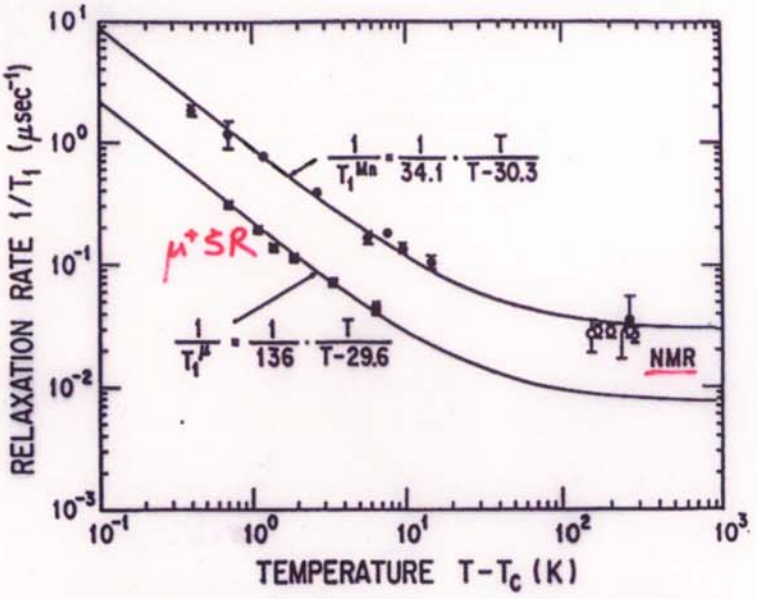

SCR - Theory
(Moriya)

Figure 3. The ^{55}Mn nuclear spin relaxation rate ($1/T_1^{Mn}$, closed circles) and μ^+ spin relaxation rate ($1/T_1^{\mu}$, closed squares) in MnSi obtained in the present ZF-μ^+SR experiment are plotted against $T - T_c$. The solid curve shows the best-fitted theoretical relaxation rate by assuming the Moriya expression Eq.(2). Also shown are the ^{55}Mn NMR data (open circles, Ref.2) for comparison.

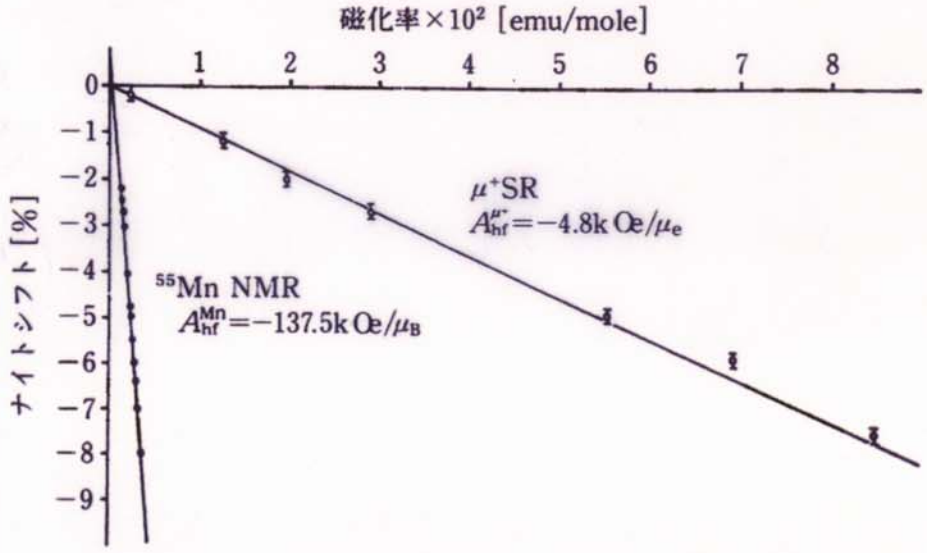

図 2.37 MnSi の μ^+, ^{55}Mn の K-χ プロット[43]

T. Matsuzaki, K. Nishiyama, K. Nagamine, T. Yamazaki et al. Phys. Lett. A123 (1987) 92.

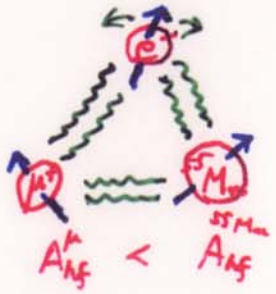

$A_{hf}^{\mu} < A_{hf}^{^{55}Mn}$

Muonium Atom in the Bloch State: A Wave of Matter (R40 and R78)

R. Kadono and W. Higemoto (KEK-IMSS), K. Nagamine and F. L. Pratt (RIKEN-RAL)

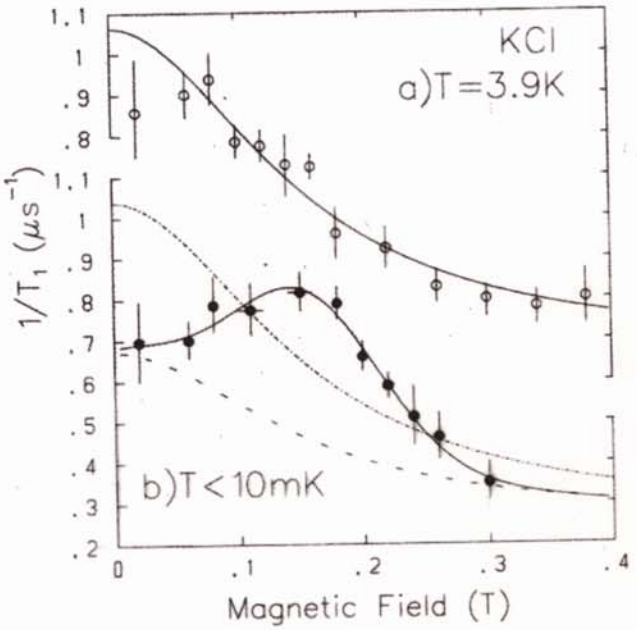

Fig. 1. Muon spin relaxation rate for muonium in KCl (a) at 3.9 K and (b) below 10 mK. For the solid curves see the text. The dot-dashed curve in (b) is the best fit to a Lorentzian spectrum, whereas the dashed curve is the Lorentzian spectral component fitted in conjunction with a Gaussian peak around 0.15 T to give the solid curve.

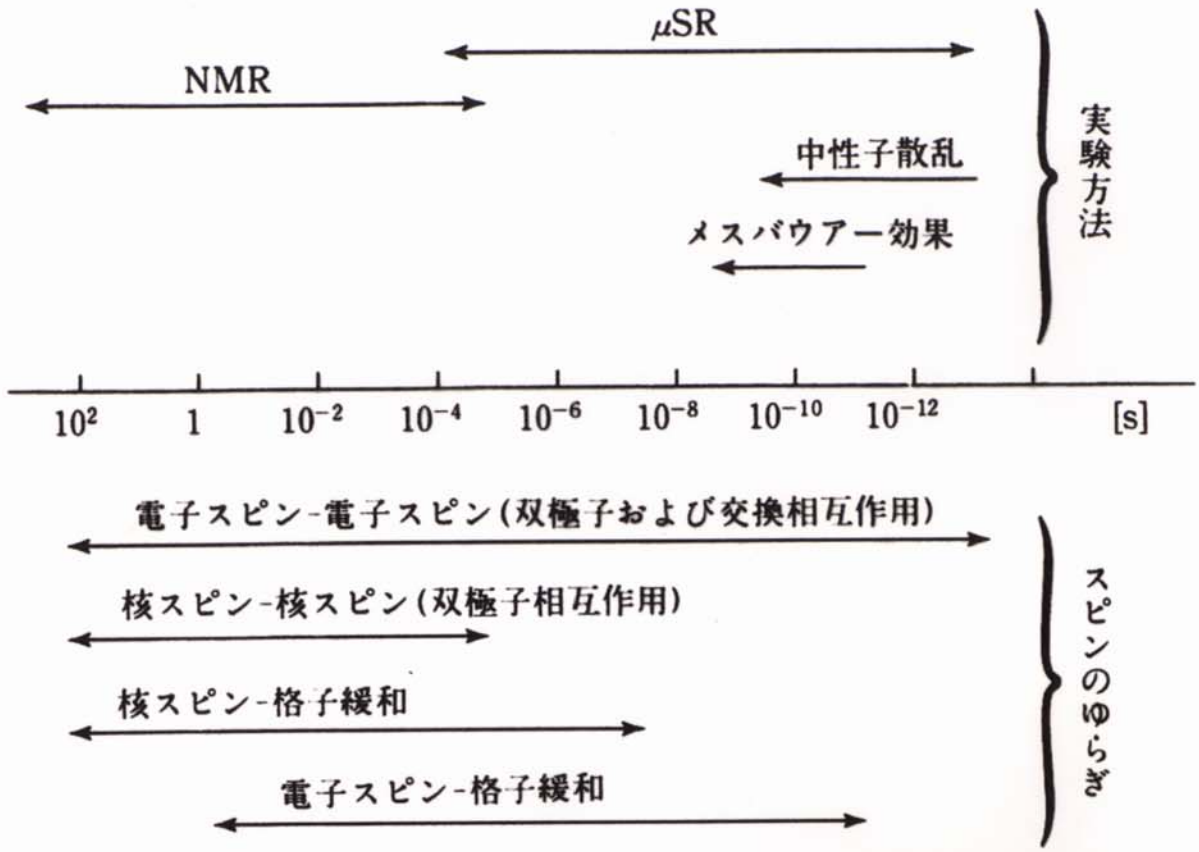

図 2.66　物質中のスピンのゆらぎの特徴的時間と測定方法

ミュオン準位交差共鳴法
μ—LCR

$$\mathcal{H} = \gamma_\mu \boldsymbol{I}\cdot\boldsymbol{B}_\mu + \gamma_N \boldsymbol{I}_N\cdot\boldsymbol{B}_N + \mathcal{H}_{\mu N}$$

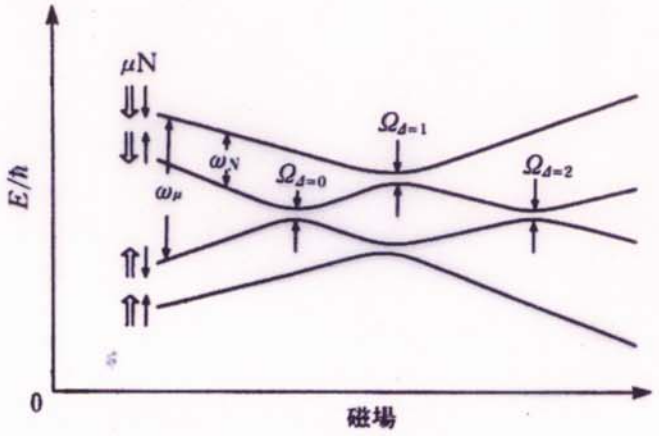

図 2.51　μ-LCR の概念図

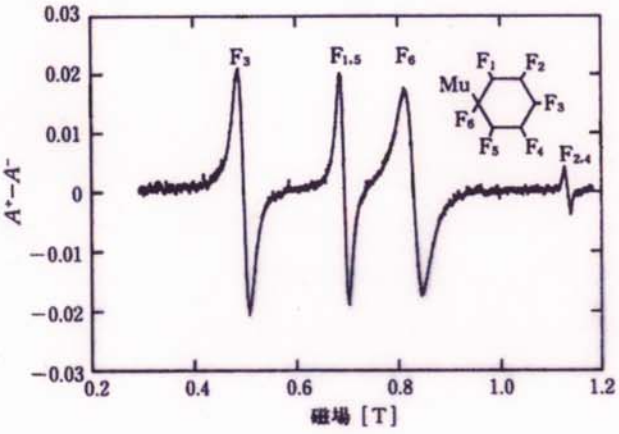

図 2.53　C_6F_6 の μ-LCR スペクトル[56]

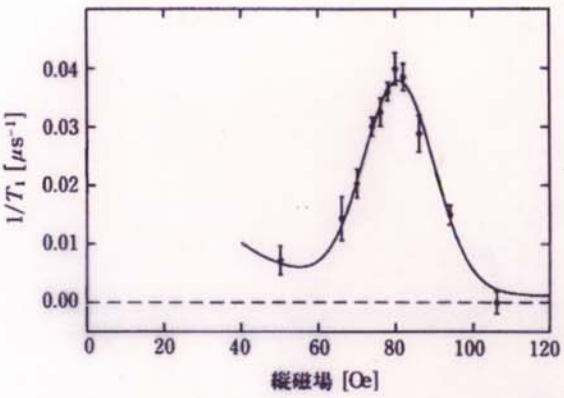

図 2.50　銅中の μ^+ の μ^+ スピン・核四重極準位交差緩和[52]

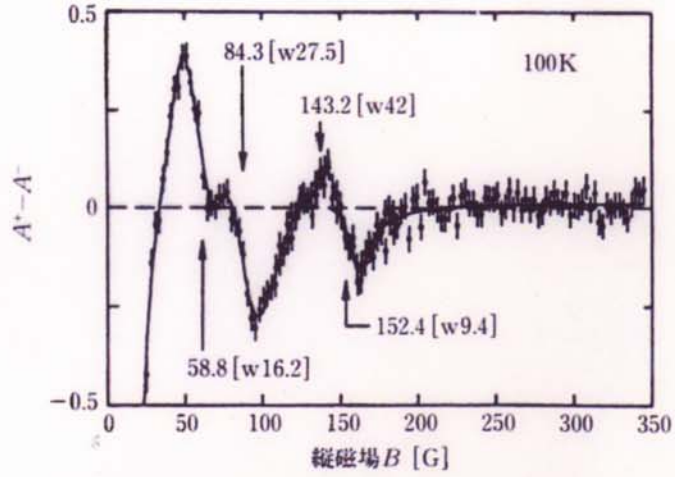

図 2.52　$YBa_2Cu_3O_7$ の μ-LCR スペクトル[55]

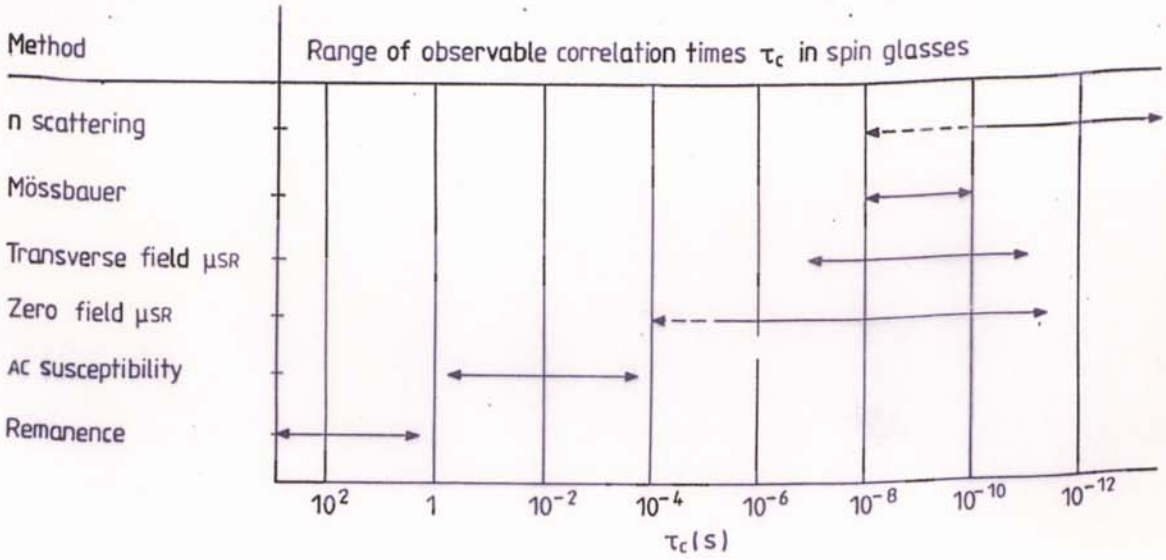

μ^+SRでは、

特有の測定の時間領域